ELSEVIER

Marine Micropaleontology 43 (2001) 155–178

MARINE MICROPALEONTOLOGY

www.elsevier.com/locate/marmicro

Late Quaternary dinoflagellate cysts from the Black, Marmara and Aegean seas: variations in assemblages, morphology and paleosalinity

P.J. Mudie[a,*], A.E. Aksu[b,1], D. Yasar[c]

[a]*Geological Survey Canada Atlantic, Box 1006, Dartmouth, NS, Canada B2Y 4A2*
[b]*Department of Earth Sciences, Memorial University of Newfoundland, St Johns, Nfld, Canada A1B 3X5*
[c]*Institute of Marine Science and Technology, Dokuz Eylül University, Haydar Aliyev Bulvar, No: 10, Inciralt, Izmir, Turkey 35340*

Received 21 July 1999; revised 17 October 2000; accepted 30 November 2000

Abstract

The link between sea surface salinity (SSS) and dinoflagellate cyst morphology was studied quantitatively in cores of Late Quaternary mud from the Black, Marmara and Aegean seas, where oxygen isotopic and planktonic foraminiferal data show salinities of about 5–19, 15–22 and 36–39 ppt, respectively. In the Black Sea, late glacial muds contain low-diversity assemblages of the cruciform species *Spiniferites cruciformis* and *Pyxidinopsis psilata*, with most *S. cruciformis* cysts having expanded septal membranes (form 1: circular outline, form 2: irregular). The assemblage is associated with surface salinities of <7 ppt. Overlying sapropelic muds have salinity estimates of ~14–18 ppt and contain *Lingulodinium machaerophorum–Spiniferites–Cymatiosphaera* assemblages, with many *L. machaerophorum* cysts having short processes and *S. cruciformis* with reduced septa (forms 3, 4 and 5). The late Holocene coccolith-rich sediments, with salinity of ~18–20 ppt, have diverse assemblages of *Brigantedinium*, *Peridinium ponticum* and other protoperidinioids, together with normal cysts of *L. machaerophorum* and *Operculodinium centrocarpum* (sensu Wall and Dale (1966), Nature 211, 1025–1026) that bear long processes.

In the northeast Aegean core, stenohaline species and morphotypes are rare, occurring only as low percentages of *S. cruciformis* forms 3 and 4, and *O. centrocarpum* var. '*truncatum*' in a mid-Holocene sapropel that was deposited during a period of high runoff and Black Sea water outflow. Marmara Sea cores record surface salinities of 14–18 ppt during late glacial sapropel deposition and 20–22 ppt for the overlying marine sediments. The sapropel is dominated by *S. cruciformis* forms 1 and 2 and by *P. psilata*, with common *L. machaerophorum* (clavate and normal forms). In surface sediments, *L. machaerophorum* is co-dominant with *O. centrocarpum* (normal and truncate forms), *Brigantedinium* and *Spiniferites* spp. Percentages of *S. cruciformis* (five forms) and *L. machaerophorum* (two forms) plotted against proxy-salinity data, however, show no clear correlation, indicating that morphological variation is not a simple function of salinity.

Keywords: sea surface salinity; Quaternary; dinocyst morphology; Black Sea; Marmara Sea; Aegean Sea

1. Introduction

There have been few previous studies (Wall and Dale, 1974; Wall et al., 1973; Duman, 1994; Aksu et al., 1995a) of Quaternary dinoflagellate cysts (= dinocysts) and acritarchs in the marginal seas

* Corresponding author. Fax: +1-902-426-4104.
E-mail addresses: mudie@agc.bio.ns.ca (P.J. Mudie), aaksu@sparky2.esd.mun.ca (A.E. Aksu).
[1] Fax: +1-709-737-2589.

0377-8398/01/$ - see front matter
PII: S0377-8398(01)00006-8

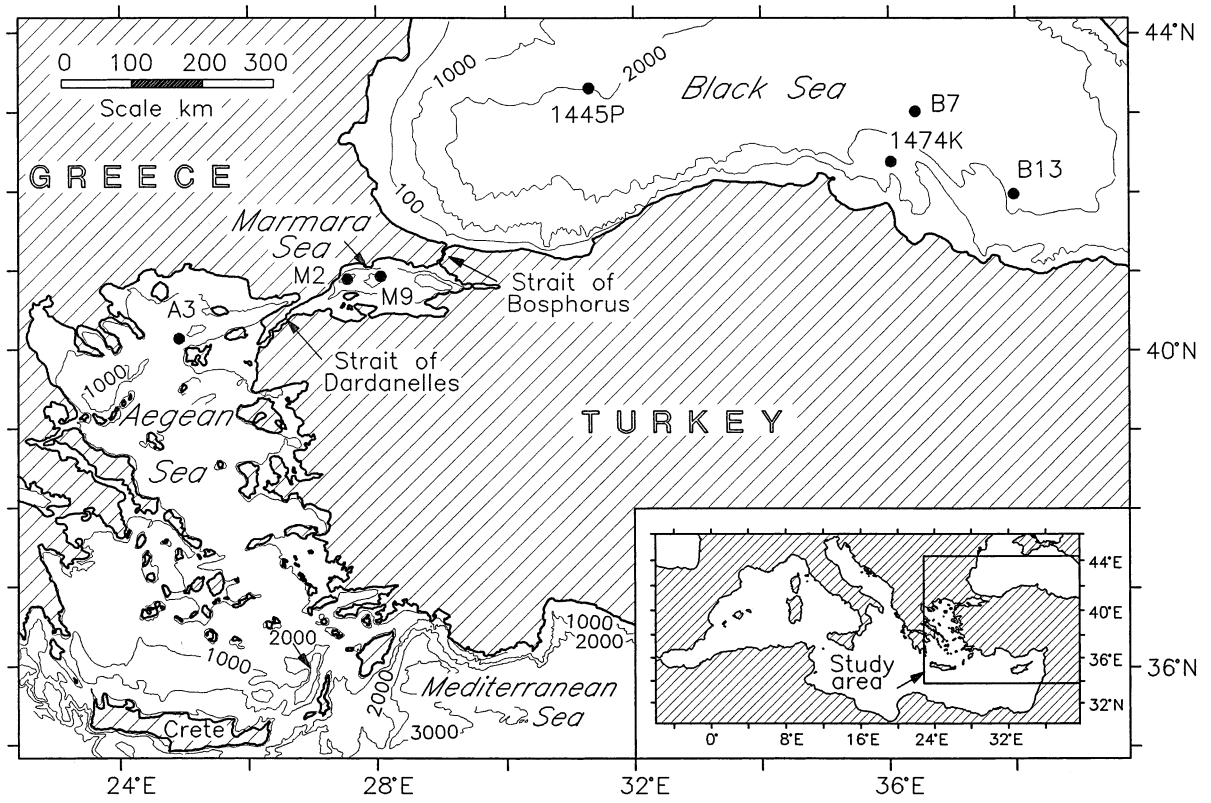

Fig. 1. Map of the eastern Mediterranean, Aegean, Marmara and Black seas, showing bathymetry and locations of core sites (after Aksu et al., 1999). Inset shows entire Mediterranean Sea.

adjoining the eastern Mediterranean: the Aegean, Marmara and Black seas (Fig. 1). The Black Sea is connected to the Aegean Sea through the Strait of Bosphorus (35 m depth), the small land-locked Marmara Sea, and the Strait of Dardanelles (65 m depth). The Aegean Sea is linked, in turn, to the Mediterranean through deeper straits (1 km depth) northwest and northeast of Crete. The straits of Bosphorus and Dardanelles restrict the exchange of water among the marine basins as evident in the very large gradient in surface water salinities (Fig. 2) found from the Black Sea (maximum ~15–21 ppt, where ppt = parts per thousand), to the Marmara Sea (21 ppt average) and the northern Aegean Sea (minimum 32 ppt immediately southwest of the Strait of Dardanelles, 34–35 ppt at the Aegean core site). The near isolation of these seas and the strong salinity gradient provide an important opportunity to study the responses of dinoflagellate cyst morphology to long-term changes in salinity, including the evolution of quasi-endemic stenohaline species, and variations in the cysts of widespread euryhaline species that may reflect large changes in salinity conditions, as suggested by previous studies (e.g. Wall and Dale, 1973; Nehring, 1994; Dale, 1996; Matthiessen and Brenner, 1996).

In this paper, the dinocyst assemblages and the morphological variations of selected species are described in Holocene cores from the southeast Black Sea, where downcore salinity estimates made by previous workers range from <7 to 19 ppt. Then, these low salinity assemblages are compared with those found in a Holocene core from the northeast Aegean Sea where downcore surface salinity estimates vary between 36 and 39 ppt. Finally, the dinocyst assemblages in two late glacial to Holocene cores from the intermediate Marmara Sea are

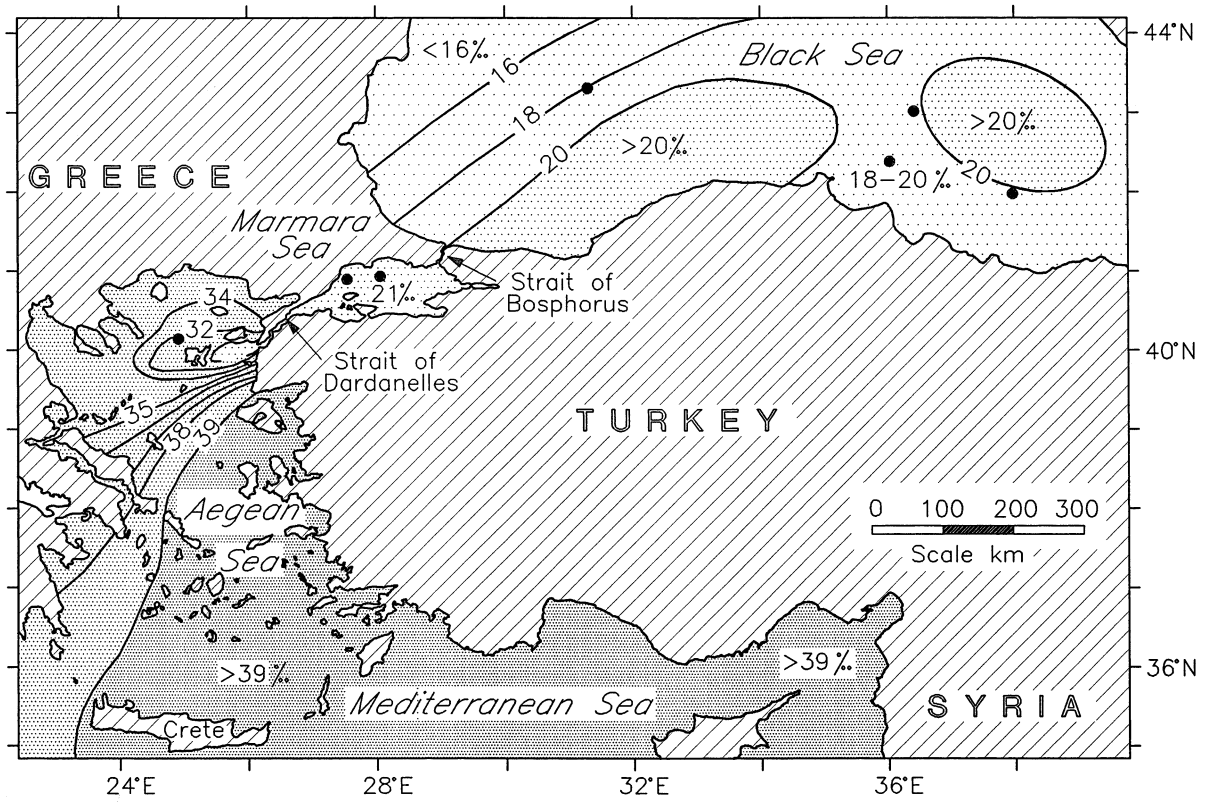

Fig. 2. Modern average surface water salinities (winter) in the study areas and adjoining seas, from Aksu et al. (1995b) and the Institute of Marine Sciences and Technology (Black and Marmara seas).

described, where the downcore salinity estimates range from 14 to 22 ppt. This is the first published report on the palynology and quantitative paleosalinity of Marmara Sea Quaternary sediments, as estimated from oxygen isotopic and planktonic foraminiferal transfer functions. Data from these cores are also used to show how the morphology of the dominant species *Spiniferites cruciformis* and *Lingulodinium machaerophorum* varies with long-term changes in salinity over a range of about 14–22 ppt. These are the first paleoecological data to examine the statistical relationship between paleosalinity estimates and variations in cyst morphology in order to test hypotheses (e.g. Wall et al., 1973; Wall and Dale, 1973; de Vernal et al., 1989; Dale, 1988, 1996; Kokinos and Anderson, 1995) that certain unusual features, such as cruciform body shape or reduced processes, are reliable indicators of low salinity paleo-environments.

2. Methods

The cores used in this study (Fig. 1) were collected from the RV Koca Piri Reis of the Dokuz Eylul University Institute of Marine Sciences and Technology, using a 4 m long wide-diameter gravity corer. All cores were stored at ~4°C until they were split, described and sampled for micropaleontological and stable isotopic studies. The sedimentology of the cores is described in detail elsewhere by Duman (1994; Black Sea), Aksu et al. (1995a,b; Aegean Sea) and Aksu et al. (1999; Marmara Sea). Methods for planktonic foraminifera and coccolith studies are described in Aksu et al., 1995; Duman (1992). Oxygen isotopic measurements were made using the only abundant planktonic foraminiferal species *Globigerina quinqueloba*, following the procedure described by Aksu et al. (1995b). Estimates of sea surface temperatures (SST) were obtained using the

Table 1
Total numbers and relative abundances of dinoflagellates, acritarchs, pollen and spores in core B7 from the southeastern Black Sea. Peridinioids include cysts of *Protoperidinium* and *Peridinium*; others are polykrikoids

Core B7: depth in cm	0	10	20	30	40	50	60	70	80	90	100	110	120
Total dinocysts/g × 1000	12	8.3	18	93	14	99	5.7	2.7	3	3	7.1	4	6.5
Total acritarch/g × 1000	12	14	12	114	9.8	6	3.9	0.3	0.2	0.2	0.1	0.1	0.2
Total pollen and spores/g × 1000	42	36	114	130	46	106	36	16	15	10	7.6	8	7
Dinocyst species													
(A) Protoperidinioids													
Brigantedinium spp.	10	8	6	10	5	1	2	0	2	0	2	0	3
Peridinium ponticum	7	2	0	3	2	1	14	6	4	0	4	0	5
Selenopemphix nephroides	3	1	0	0	0	0	6	0	0	0	0	0	0
S. stellatum	2	3	4	0	0	1	0	0	0	0	0	0	0
Polykrikos kofoidii	3	1	2	1	2	0	0	0	0	0	0	0	0
(B) Gonyaulacoids													
Gonyaulax tamarensis	0	3	10	28	9	1	0	0	0	0	0	0	0
Lingulodinium machaerophorum	9	9	10	10	17	37	2	0	2	0	0	0	0
Operculodinium centrocarpum	0	4	4	12	16	15	2	2	2	0	0	0	0
Spiniferites bentorii	1	1	4	6	4	2	6	0	0	0	0	0	0
S. cruciformis form 1–4	0	0	0	2	2	5	0	22	30	20	10	15	10
S. cruciformis form 5	1	0	2	4	1	3	0	48	50	60	84	80	80
S. inaequalis	1	1	2	1	0	4	0	2	1	0	0	0	0
S. mirabilis	0	1	4	3	9	3	0	0	0	0	0	0	0
Spiniferites spp.	7	3	16	9	18	15	32	2	3	0	0	0	0
Pyxidinopsis psilata	1	2	0	0	0	0	0	0	0	0	0	0	0
Acritarchs													
Cymatiosphaera globulosa	25	33	24	7	10	4	22	8	4	0	0	0	0
Pollen and spores													
Abies	3	0	1	2	1	0	0	0	1	0	0	0	1
Cedrus/Pinus	17	20	18	16	13	14	10	7	6	5	7	6	6
Cupressaceae	6	5	7	3	3	2	0	13	10	3	0	5	2
Ephedra	1	0	1	1	0	0	0	0	0	0	0	0	0
Picea	1	1	0	0	2	0	0	0	0	1	1	0	1
Alnus	16	9	15	13	12	13	30	4	4	3	3	4	4
Artemisia	2	8	7	14	10	5	6	14	18	20	22	20	23
Betula	5	4	3	4	2	7	4	4	3	1	2	1	3
Carpinus/Ostrya	12	6	4	5	1	5	7	4	2	3	2	2	2
Chenopodiaceae	2	3	4	6	3	2	7	8	10	12	14	12	15
Compositae	0	3	0	2	0	0	2	2	5	3	7	4	3
Corylus	1	4	2	0	2	4	4	1	2	1	1	1	2
Ericales	1	1	1	1	0	0	0	0	0	1	0	1	0
Gramineae	6	8	11	3	4	5	3	7	10	7	10	8	10
Fagus	2	8	0	9	7	9	2	2	1	1	1	1	1
Olea	3	2	2	1	0	0	0	0	0	0	0	0	0
Papaveraceae	3	1	2	1	0	0	0	0	0	0	0	0	0
Pterocarya	5	3	5	2	7	7	6	1	1	0	0	1	0
Quercus	8	6	3	12	15	10	2	13	14	16	17	14	19
Rosaceae	3	1	1	2	1	2	2	6	3	4	6	5	1
Tilia	1	3	0	0	0	1	0	3	2	1	0	1	0
Ulmus	2	0	1	1	4	4	5	0	1	0	1	1	2
Filicales	0	1	0	0	2	0	3	5	6	5	5	6	5

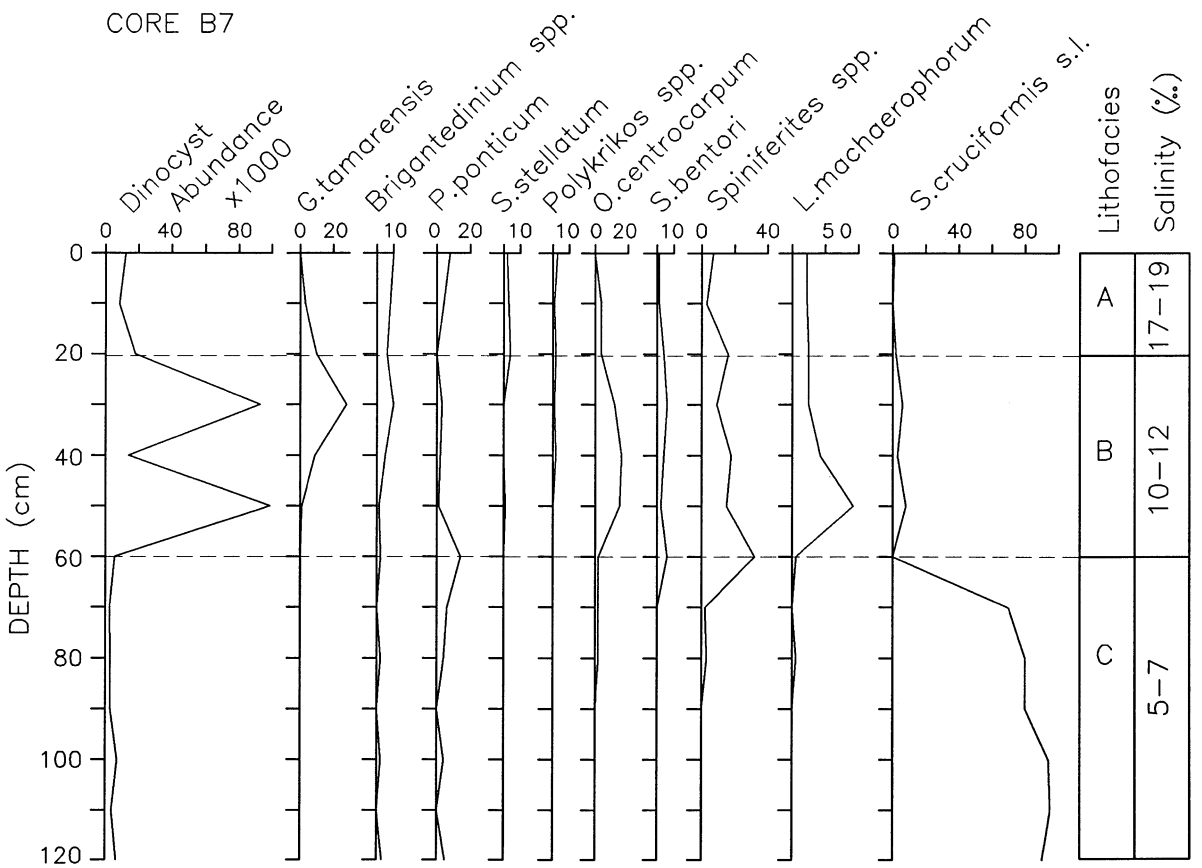

Fig. 3. Black Sea core B7, showing lithofacies, estimated paleosalinity in parts per thousand (‰) as reported by Wall and Dale, 1973, dinocyst abundance per cm^3, and percentage abundance of the main species.

Mediterranean-based planktonic foraminiferal varimax description matrix and the corresponding transfer function of Thunell (1979). The oxygen isotopic composition of the surface water ($^{18}O_w$) was calculated using the temperature equation of Shackleton (1974) as described in Aksu et al. (1995b). The downcore sea surface salinities were calculated using the linear regression equation between the salinity and oxygen isotopic composition of waters in the Aegean and Marmara seas, using the method of Aksu et al. (1995b). This Mediterranean-based transfer function method apparently overestimates the Aegean Sea sea surface salinity (SSS) by up to 3 ppt, but this is well within the range of observed annual salinity fluctuations (31.5–39 ppt) at the core site (Yasar, unpub.).

Palynomorphs were extracted from samples of 2–5 cm^3 volume, using standard methods for Quaternary marine sediments (Mudie, 1982): sieving at 10 and 125 μm mesh sizes, digestion in HCl and HF, and adding exotic spores to obtain estimates of palynomorph concentration per cm^3. Except where noted, species names are the same as those of Williams et al. (1998) who give the authorship and references to the names.

3. Results

3.1. Black Sea assemblages

Cores B7 and B13 were recovered from water depths of 2120 and 2050 m, respectively (Fig. 1), about 100 km east of the core sites 1474 and 1475

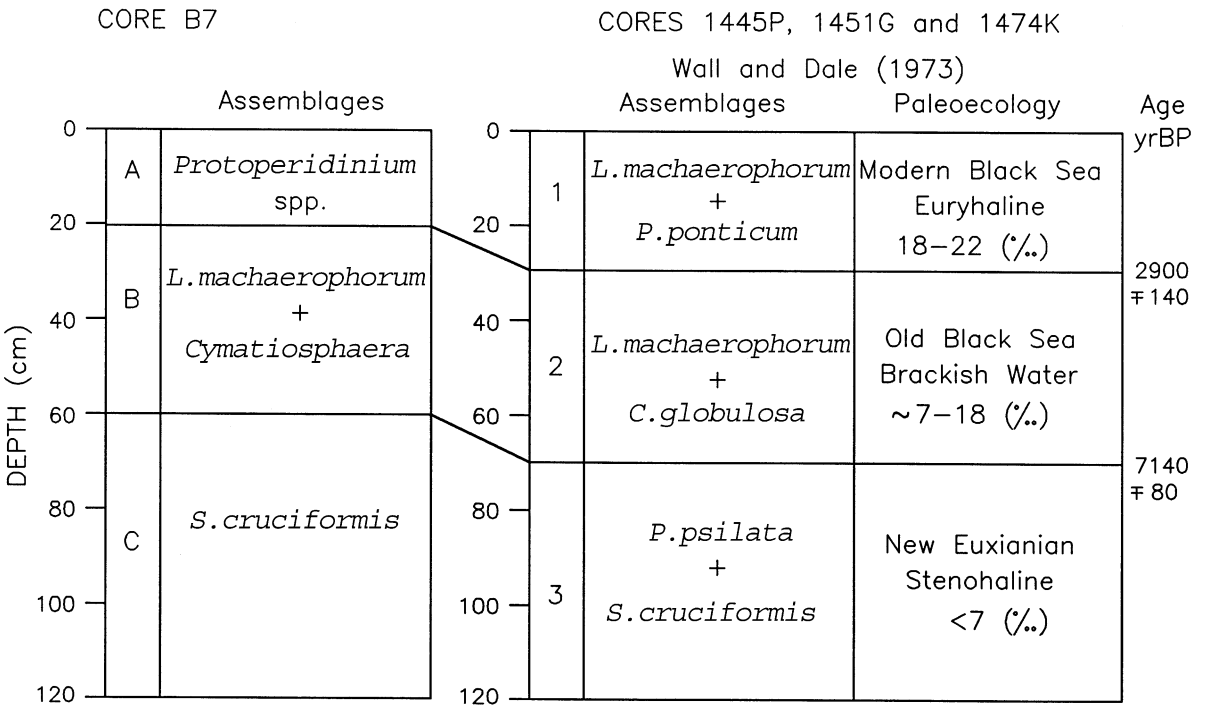

Fig. 4. Correlation between lithofacies (A–C; 1–3) and palynomorph assemblage zones in cores B7 (this study) and 1451G of Wall and Dale (1973), using Wall and Dale's chronology and salinity estimates in ppt (‰) derived from this paper.

studied by Wall and Dale (1973, 1974). Cores B7 and B13 contain the same dinocyst and pollen assemblages (Mudie, unpublished data) except in a ~20 cm-thick upper Holocene turbidite in the upslope core B13. Only Core B7, which is almost turbidite free (Duman, 1994) is discussed in detail here. The dinoflagellate cysts, acritarchs and relative abundances of pollen and spores found in Core B7 are listed in Table 1.

Core B7 contains three lithofacies (Fig. 3), which correspond closely to facies 1–3 at Wall and Dale's sites 1474K, 1445P and 1451G (Fig. 4). Two intervals in core 1474K were radiocarbon dated and the sediments in this core were cross-correlated with ^{14}C-dated lithofacies in core 1462 (Ross et al., 1970), and with the well-dated European pollen chronology (Wall and Dale, 1973; Wall et al., 1973). However, the reported ^{14}C ages for facies boundaries vary by up to 2000 yr from one report to another (see Table 4 in Wall and Dale, 1974; also discussions in Crusius and Anderson, 1992; Jones and Gagnon, 1994) and it is known that the variable reservoir effect and contamination by old carbon are problem in precise dating of Black Sea sediments. For ease of comparison with previous Black Sea studies, we continue to use the uncorrected ^{14}C ages of about 7000 and 3000 yr BP for the base and top of Unit 2 because we are not attempting to measure rates of cyst deposition. However, varve counts of Duman (1994) suggest that the ages of the sapropel may be up to 3000 yr younger than the reported ^{14}C ages, if the laminae in this unit represent annual deposits, while Jones and Gagnon (1994) give a corrected carbonate carbon age of 7540 ± 130 yr BP. These uncertainties are still under investigation, but they are not crucial to this paper because any further age correction does not prevent general comparison of the dinocyst assemblage characteristics or their correlation with surface water salinities.

Facies C at the base of core B7 contains a 70 cm-thick olive-gray mud unit with discontinuous silt laminae, similar to Unit 3 in cores 1474K and 1445P. Litho- and palynostratigraphic correlations with core 1474K suggest that the top of Facies C in

core B7 is ~7000 yr old, while the abundance of oak pollen indicates that the base of core B7 at 1.2 m depth must be <9000 yr BP. Oxygen isotopic measurements on calcitic carbonate (Deuser, 1972) indicated that the salinity of the Black Sea during the deposition of Unit 3 was ~5–7 ppt, while ion diffusion studies (cited by Deuser, 1972) indicated a lower, more or less constant salinity of ~3.5 ppt from 20,000 to 8000 yr BP. Unlike the longer Unit 3 (11 m, ~23,000 yr BP) studied by Wall and Dale (1974), reworked pre-Quaternary palynomorphs are rare or absent in Facies C of core 7B, which probably corresponds only to the uppermost post-glacial interval of their unit.

Facies C contains a relatively low abundance of 3000–6500 dinocysts cm^{-3} (Fig. 3; Table 1), comprising a very low diversity flora with 2–5 species that is similar to the 'freshwater' New Euxinic Stage assemblage of Wall and Dale (1973). The assemblage is dominated (~80%) by *S. cruciformis* and spherical cysts of *Pyxidinopsis psilata*, with rare *Peridinium ponticum* and *Brigantedinium* spp. except at the top where other gonyaulacoids (*Spiniferites bentorii*, *S. inaequalis* and *Operculodinium centrocarpum*) increase to ~40%. Head (1994) found that the larger cruciform morphotypes assigned to *P. psilatum* by Wall et al. (1973) are actually detached endocysts of *S. cruciformis*. We agree with this and we have included all large (>45 μm) cruciform or biconical cysts with granulate surface ornament and traces of paratabulation in *S. cruciformis* (as *S.c.* form 5, see Plate I, Fig. 1). In our samples, *P. psilatum* differs by its smaller size (30–45 μm), spherical shape and smooth or scabrate wall surface that lacks paratabulation. The thecate stage of *S. cruciformis* is unknown, but the cyst morphology strongly suggests an origin from *Gonyaulax spinifera* (see Eaton, 1996). In contrast, Dale (1996) reports that smooth, nontectate *P. psilata* cysts from the Baltic Sea excyst to produce *Protoceratium reticulatum* which is also the thecate stage of *O. centrocarpum* sensu Wall and Dale, 1966.

The assemblages from early Holocene sediment in cores B7 and 13 show a wide range of morphological variation in *S. cruciformis* (Plate I), as also described and illustrated by Wall et al. (1973) for the upper part of their Unit 3 (~7000–13,000 yr BP). The variation includes the degree of development of sutural septa, process length and branching, and the appearance of membranous flanges (entire to perforate). Precise measurement of these parameters for specimens from a wider range of low salinity environments (say, 0–5 ppt) may show that there is a continuous gradation in the expression of these characters. In the brackish water to estuarine environments of the Black and Marmara seas, however, five groups of morphotypes can be distinguished during routine counting. The main features of these morphotypes (referred to as forms) are outlined below.

S. cruciformis form 1 (Plate I, 10–12). A large, subcircular morphotype: cyst diameter ~65–80 μm, with an almost circular outline in dorso-ventral view (note that all the forms are dorso-ventrally flattened and rectangular to oval in polar or side view). The rounded outline is defined by the presence of long (9–22 μm) gonal processes, many of which are connected by wide membranous sutural septa and expanded flanges. The endocyst (~45 × 40 μm) has a scabrate to finely granular surface and is strongly rounded-cruciform on account of concave pre- and post- cingular lateral sides. Sutural ridges are well developed except in the ventral area, and are expanded into elevated septa in lateral and polar areas. All processes are strongly developed (30–50% of the maximum body width), with widely divergent bifurcate (rarely trifurcate) tips; some processes are joined by membranous flanges to form box-like structures; others are connected by perforated sutural membranes. This morphotype superficially resembles *Seriliodinium explicatum* because of the expanded perforate septa and flanges, but it lacks trabeculae linking gonal process tips, encircling the cysts and forming very large fenestrations.

S. cruciformis form 2 (Plate I, 7,8). A large morphotype with an irregular, asymmetrical cyst outline: widest cyst diameter 60–70 μm, with a cruciform endocyst (45–40μm) and long (10–22 μm) processes similar to form 1 but with an irregular outline because development of the membranous septa and flanges is restricted to the ventral posterior and apical areas, and because the left lateral flange is often much larger than on the right. Most of the septa are imperforate in this form.

S.cruciformis form 3 (Plate I, 4,5,9). A large spinose morphotype: cyst diameter 60–70 μm, with

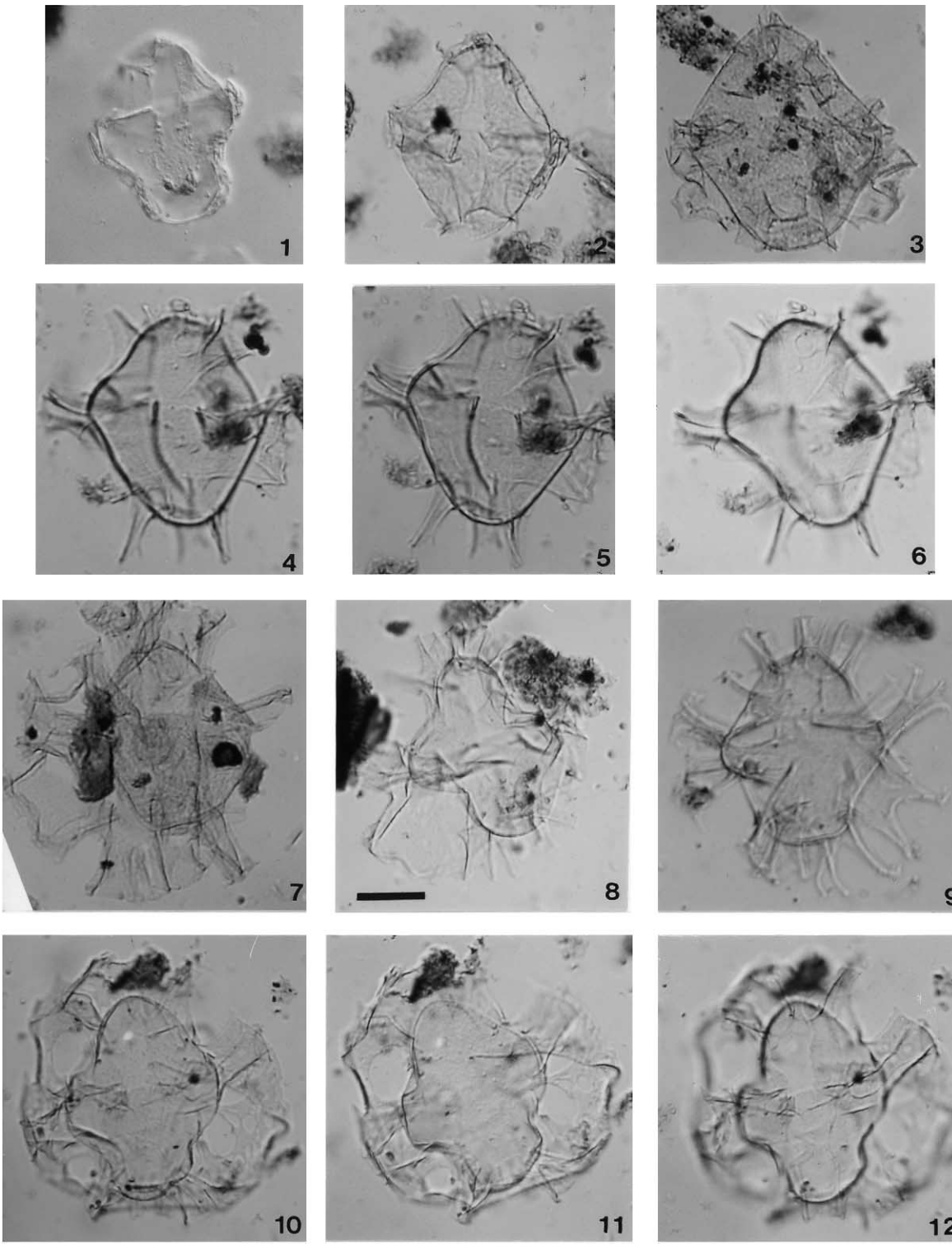

Plate I.

a large cruciform to biconical endocyst (45–40 μm). Processes are well developed (18–20 μm) and joined by low septa (<5 μm) so that the cyst has a spiny (not rounded) appearance in dorso-ventral view. Occasionally, the posterio-ventral processes are joined by expanded septa.

S.cruciformis form 4 (Plate I, 2,3). A smaller morphotype (50–60 μm), sometimes with less concave endocyst sides, and with short (5–8 μm) or nodular (<5 μm) processes. Sutural septa are absent, low or almost as wide as the processes in the posterio-ventral area. The short (<5 μm) processes may be rigid with expanded septa, membranous or crumpled into nodules.

S. cruciformis form 5 (Plate I, 1). A smaller morphotype (45–55 μm) because of the absence of processes. This form has strongly cruciform to biconical cysts with scabrate to granular surface ornament and is the same size as the endocysts of the other forms. Septa are absent but sutural ridges are present, often with nodules apparently corresponding to vestigial gonal processes. As first pointed out by Head (1994), this cyst-form was lumped with cruciform morphotypes of *Tectatodinium psilatum* (now *P. psilata*) by Wall et al. (1973). In our samples, however, *S. cruciformis* form 5 is consistently larger than *P. psilata*, which has a cyst size of 30–45 μm, is spherical with a smooth or scabrate wall, and lacks any traces of paratabulation.

In cores B7 and B13, *S. cruciformis* forms 1 and 2 are most common in Facies C, with less than 20% of the other forms present except at the top where all forms rapidly decrease and where *P. ponticum* increases to 10–15%. Isotopic data from Core 1474K (Deuser, 1972) suggest that surface water salinity increases in this interval, but few proxy-salinity measurements were made and it is not possible to quantify the statistical relationship between cyst morphology and salinity in the early Holocene Black Sea assemblages. There is also insufficient evidence to determine if salinity increased slowly or in pulses during the early Holocene, as suggested by large variations of cyst abundance found in cores studied by Wall and Dale (1973). In Core B7 (Fig. 3), the increase in *P. ponticum* may mark a transitional assemblage zone similar to the low diversity *O. centrocarpum–Spiniferites bulloideus–P. psilata* assemblage found in recent sediments of the southern Baltic Sea (Matthiessen and Brenner, 1996), where the average salinity is 6–7 ppt, with a maximum of 9.35. However, the virtual disappearance of *S. cruciformis* and *P. psilata* at the base of Unit 2 suggests the inability of these stenohaline taxa to survive an apparently abrupt salinity change at ~7000 yr BP to values of 10–12 ppt (Deuser, 1972) or more (7–18 ppt is suggested by Wall and Dale, 1973).

Facies C in Cores B7 and B13 is overlain by a 35 cm-thick laminated sapropelic mud unit (Facies B) which clearly correlates with Unit 2 of Wall and Dale (1974) and has an age of ~7000–3000 yr BP. Isotopic data suggest ~10–12 ppt salinities for this interval (Deuser, 1972). Dinocysts are very abundant (20,000–80,000 cm^{-3}), with the assemblage being dominated by euryhaline species (Rochon et al., 1999), such as *L. machaerophorum*, *O. centrocarpum* sensu Wall and Dale, 1966, *S. bentorii* and *S. ramosus*. Cysts resembling the resting spores of *Gonyaulax tamarensis* (see Simard and de Vernal, 1998) are also present in low numbers. The acritarch species *Cymatiosphaera globulosa* is abundant (Table 1) in Facies B, as found in Unit 2 of Wall and Dale's cores. In cores B7 and B13, cysts of heterotrophic (diatom-feeding) protoperidinioids and polykrikoids increase (*Brigantedinium* spp., *Stelladinium stellatum*, *Polykrikos kofoidii*) and the common northeast Atlantic species *Spiniferites mirabilis* makes its first appearance. The stenohaline species *P. psilata*

Plate I. Light microscope photographs of *S. cruciformis* morphotypes from Core M9, 100 cm depth (most figs) and Core B7, using interference contrast at magnification ×400. Scale bar is 20 microns. HI, MID and LO indicate high, middle and low focal depths, respectively. GSCA curation numbers are in parentheses; England Finder co-ordinates for illustrated specimens can be obtained by request. (1) *S. cruciformis* form 5: HI, dorsal surface with nodule-like processes (9515-28, 50 cm). (2,3) *S. cruciformis* form 4. (2): HI, ventral surface with short processes and low septa (980529-32); (3): HI, dorsal surface with short processes and locally expanded septa (980529-31). (4–6,9) *S. cruciformis* form 3. (4–6): MID, HI dorsal and LO ventral views of well developed processes and low septa (980530-10,11,12); (9): HI, ventral surface (980530-18). (7,8) *S. cruciformis* form 2. (7): HI, dorsal surface (980529-19); (8): MID, showing discontinuous expanded septa (980529-33). (10–12) *S. cruciformis* form 1. (10): MID, with circular outline of expanded perforate septa (980529-34); (11,12): HI ventral and LO dorsal surfaces of cysts almost encircled by expanded septa (9502-04, -05).

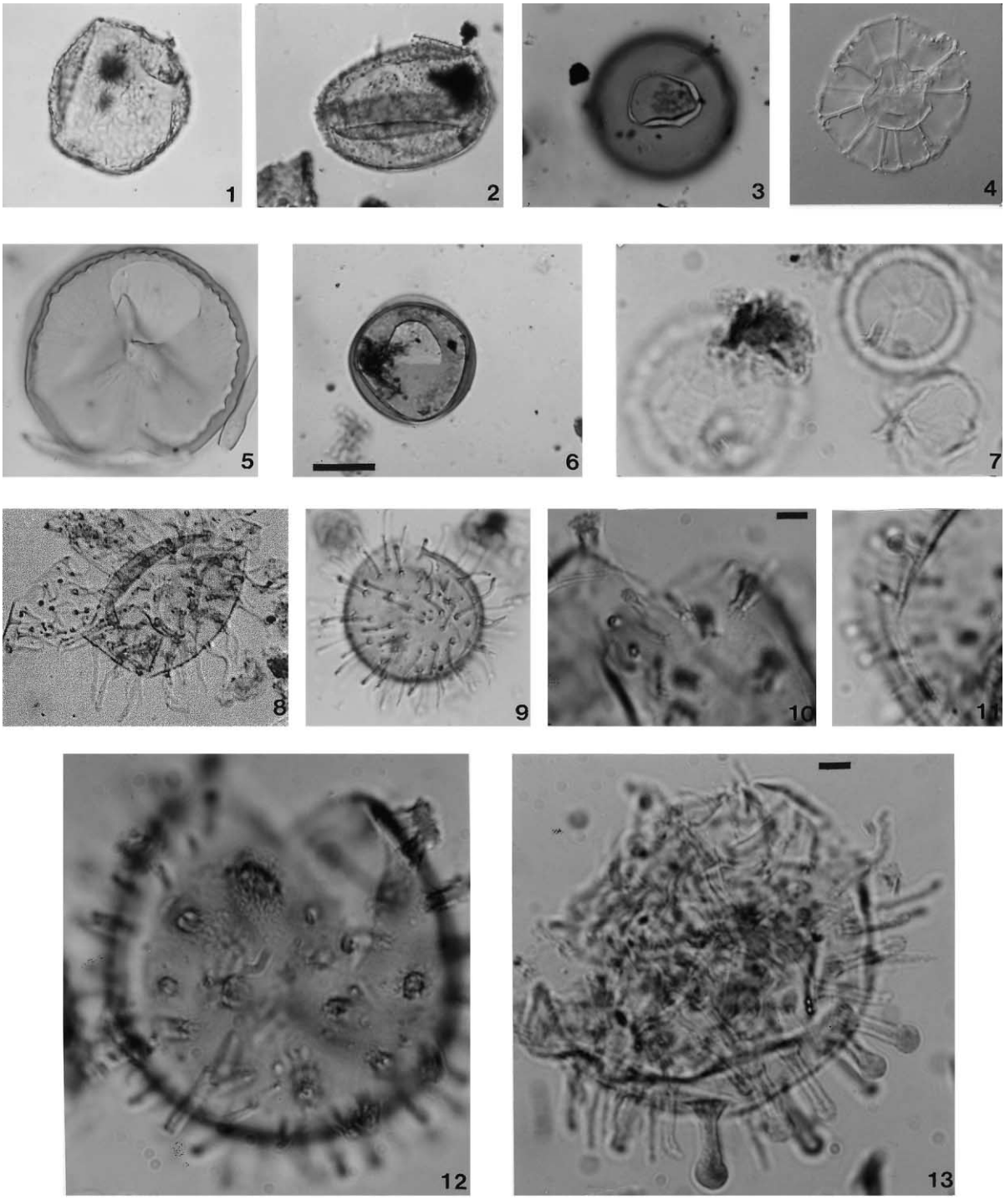

Plate II.

and *S. cruciformis* are still present but in low abundances (<10%), and *S. cruciformis* is represented mostly by forms 3 and 4. The processes of *L. machaerophorum* are quite variable in length and shape (Plate II) and include the range of morphology first illustrated by Harland (1977) for North Sea-British Isles specimens, except that all morphotypes in our samples show some development of spine shafts. Likewise, process length is variable in *O. centrocarpum* (1–8 μm), with most cysts having uniformly long spines (6–8 μm) and some with spine lengths varying from about 1–6 μm on the same cyst, but no cysts were seen with short truncate spines (*O. centrocarpum* var. '*truncatum*' of Mudie 1980, 1982).

The surface Facies A in cores B7 and B13 is a varved coccolith-rich mud for which isotopic data (Deuser, 1972) indicate salinities of 17–19 ppt. These isotopic salinity estimates are in close agreement with present-day surface salinities (Fig. 2), although values of 18–22 ppt are cited by Wall and Dale (1973). Dinocyst abundances of 10,000 cysts cm^{-3} are much lower than in the mid-Holocene sapropel. Heterotrophic protoperidinioids dominate the assemblages (*Brigantedinium* spp., *P. stellatum*, *Selenopemphix quanta*, *S. nephroides*), together with *P. ponticum* and various morphotypes of *L. machaerophorum* and *O.centrocarpum*. Above the base of the facies, *S. cruciformis* is absent and *P. psilata* is rare. This assemblage zone is similar to the *L. machaerophorum–P. ponticum* zone of Wall and Dale (1974) which was described as comprising mostly cosmopolitan, euryhaline species of common marine genera.

3.2. North Aegean assemblages

Core A3 was recovered from the North Aegean Trough in 685 m water depth, about 100 km west of the low salinity plume of Black Sea water outflow through the Strait of Dardanelles. The lithofacies and general micropaleontology of this and other Aegean Sea cores are described elsewhere (A3 = Core 3 of Aksu et al., 1995a,b,c), and the paleoecological affinity of the palynological assemblages is discussed in Aksu et al. (1995b). Here, the three dinocyst assemblage zones (Fig. 5) are described and their relation to the surface water salinity and the Black Sea zones are discussed.

Lithofacies D in core A3 is a gray-brown mud of late glacial (~12,000–10,500 yr BP) and early Holocene age (10,500–8500 yr BP). Oxygen isotopic and foraminiferal transfer function data show surface water salinities of ~37–38 ppt, and dinocyst assemblages (Table 2) are dominated by cold-tolerant euryhaline (Rochon et al., 1999) gonyaulacoids: *Nematosphaeropsis labyrinthus*, *S. ramosus*, *S. delicatus*, *S. membranaceus* and *L. machaerophorum* with long spines (e.g. Plate II, Fig. 8). Mediterranean and North Atlantic species characteristic of hypersaline estuarine and oceanic waters (see McCarthy and Mudie, 1996; Wall et al., 1977) are rare, including *Polysphaeridium zoharyi*, *Operculodinium israelianum*, *Impagidinium patulum* and *I. aculeatum*. Similar assemblages dominated by *N. labyrinthus* have been described for late glacial sediments off the Rhone Delta (Morzadec-Kerfourn, 1986).

The transition from Facies D to C (sapropel S1; 9500–6400 yr BP) is marked by a 2 ppt decrease in surface water salinities in northern Aegean Sea that corresponds to increased outflow of Black Sea water during the final disintegration of the European and Siberian ice sheets, and the breaching of the Bosphorus and Dardenelles sills by

Plate II. Light microscope photographs of indicator species from the Black Sea (1,6,7), Aegean Sea (2–5) and morphotypes of *L. machaerophorum* from Core M97-2 (11,12), using interference contrast at magnification × 400 (1–9; scale = 20 microns) or × 1000 (10–13; scale = 5 microns). HI, MID and LO indicate high, middle and low focal depths, respectively. GSCA numbers are in parentheses; England Finder coordinates for illustrated specimens can be obtained by request. (1) *P. ponticum*; MID, orientation unknown (951215). (2) *Operculodinium israelianum*; HI, on dorsal archaeopyle (980529-11). (3) *Brigantedinium simplex* HI on attached operculum. (4) *Nematosphaeropsis labyrinthus* MID, showing well-developed, straight gonal processes (981515-30). (5) *Selenopemphix nephroides* HI, on intercalary archeopyle (980403-24). (6) *P. psilata* HI on dorsal archaeopyle (980529-12). (7) *C. globulosa* MID, showing reticulate ornament (980529-29). (8–11) *L. machaerophorum* morphotypes. (8) Cyst with long, mostly aculeate spines (980529-20?). (9) Cyst with long, thin clavate spines (980529-23). (10–13) *L. machaerophorum* II 'clavate' form. (10,12) Cyst with narrow and conical-based spines with blunt tips (980529-29); (11,13) Cysts with mixed straight, acuminate and conical spines with swollen round tips; note variable lengths of the processes from <5 microns (11, 98052925) to ~10 microns (13, 98052926).

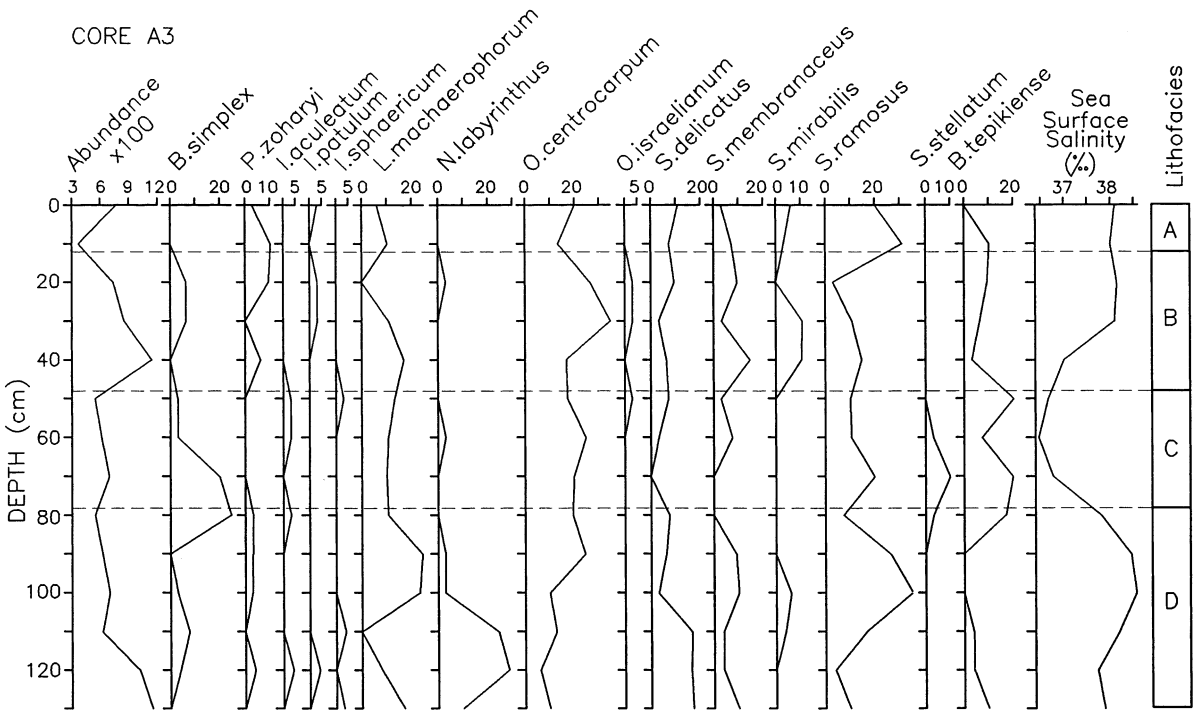

Fig. 5. Aegean Sea core A3, showing lithofacies, paleosalinity in ppt (‰), dinocyst abundance cm^{-3}, and percentage abundances of main species (after Aksu et al., 1995b).

rising sea level (Aksu et al., 1995a,b, 1998). At the base of Facies C, the dinocysts are dominated by the protoperidinioids: *Brigantedinium simplex* and *S. stellatum*, with *P. ponticum* being occasionally present. Gonyaulacoids are mainly *Bitectatodinium tepikiense*, which favors well-stratified temperate waters, *L. machaerophorum* (long spines), *O. centrocarpum*, including *O. centrocarpum* var. '*truncatum*', and *S. ramosus*. Rare specimens of *S. cruciformis* form 2 were also found in this unit. This northeast Aegean assemblage zone thus has some features in common with the sapropelic unit in the Black Sea cores and it differs significantly from the *Brigantedinium*-dominated mid-Holocene assemblages described for the Alboran (Turon and Londeix, 1988) and the Adriatic (Zonneveld, 1995) seas of the western Mediterranean.

The youngest lithofacies (B and A) in core A3 are carbonate-rich muds with relatively high salinities averaging 38–39 ppt (Aksu et al., 1995b). The dinocyst assemblage is dominated by gonyaulacoid species commonly found in modern sediments of the Northeast Atlantic and the Mediterranean Sea: *S. ramosus*, *S. mirabilis*, *S. membranaceus*, *L. machaerophorum* and *O. centrocarpum* with long spines, *O. israelianum* and *P. zoharyi*. The last two tropical species decrease in Facies A (0–3 cm, 440 yr BP), perhaps in response to the Neoglacial cooling.

3.3. Marmara Sea assemblages

Cores M9 and M97-2 were recovered from water depths of ~1200 m in the western and eastern basins of Marmara Sea, respectively. Lithofacies C in core M9 has uncorrected accelerated mass spectrometry (AMS) radiocarbon ages of 21,950 ± 310 yr BP (TO5367) and 29,540 ± 1540 yr BP (TO5369) for shells extracted from 40 cm and 215 cm depth in the core, respectively. The first occurrence of *P. stellatum* at 30 cm (Table 3) suggests that the top of this core overlaps with the base of core M97-2 which has an uncorrected AMS ^{14}C age of 3490 ± 50 yr BP for foraminifera extracted from 210 cm in the core. Tables 3

Table 2
Total numbers of palynomorphs and relative abundances of dinoflagellates in core A3 from the Aegean Sea. Peridinioids include cysts of *Protoperidinium* and *Peridinium*

Core A3: depth in cm	0	10	20	30	40	50	60	70	80	90	100	110	120	130
Total dinocysts/g × 100	7.7	3.7	7.4	8.5	11	5.5	6.2	6.9	5.5	6.4	7	6.3	10	11
Total acritarch/g × 100	0	0	0	0	1	1	0	0	0	0	0	0	0	0
Total *Pediastrum*/g	0	0	0	0	0	18	0	0	0	0	0	141	132	38
Total pollen-spores/g × 100	2.6	3.7	4.8	7.1	9.2	17	13	68	30	2.6	2.3	2	4.4	7.2
Dinocyst species														
(A) Protoperidinioids														
Brigantedinium simplex	0	0	6	6	0	3	3	20	23	0	3	6	4	0
Brigantedinium spp.	9	0	0	3	10	7	7	0	0	0	0	0	0	0
Selenopemphix quanta	0	0	0	0	3	0	0	0	0	0	0	0	0	0
Peridinium faeroense	9	3	0	0	0	0	0	0	0	0	0	0	0	3
P. ponticum	0	0	0	0	0	0	0	0	4	0	0	0	4	0
Pyxidinopsis spp.	0	0	0	3	0	0	0	0	0	0	0	3	0	0
Selenopemphix nephroides	0	3	0	3	0	0	7	0	0	3	0	0	4	3
S. stellatum	0	0	0	0	0	0	3	10	3	0	0	0	0	0
Trinovantedinium applanatum	9	0	3	0	0	0	0	0	0	0	0	0	4	0
(B) Gonyaulacoids														
Achomosphaera andalousiensis	3	0	0	0	0	0	0	0	0	0	0	0	0	0
Ataxiodinium choane	0	0	0	0	0	0	0	0	3	0	0	0	0	0
Bitectatodinium tepikiense	0	10	9	6	3	20	7	20	16	0	0	3	4	10
Gonyaulax tamarensis	0	0	0	3	0	0	0	0	0	0	0	0	0	0
Lingulodinium machaerophorum	6	10	0	10	16	13	10	10	10	24	23	0	8	17
Nematosphaeropsis labyrinthus	0	0	3	0	0	0	3	0	0	3	3	19	28	10
Operculodinium centrocarpum	20	13	25	32	16	17	23	20	18	24	10	10	6	10
O. centrocarpum var. *truncatum*	0	0	0	0	3	0	3	0	3	0	0	0	0	0
O. israelianum	0	0	3	3	0	3	0	0	0	0	0	0	0	0
Polysphaeridium zoharyi	3	10	9	0	6	0	0	0	3	3	3	0	4	0
Spiniferites bentori	0	0	0	0	0	3	0	0	0	0	0	9	0	0
S. bulloideus	0	0	6	0	0	3	0	0	3	0	3	0	4	0
S. cruciformis	0	0	0	0	2	5	0	22	3	0	0	0	4	0
S. delicatus	11	7	9	3	6	7	3	0	7	6	3	13	16	12
S. membranaceus	3	7	9	3	14	3	7	0	0	9	10	3	4	10
S. mirabilis	6	3	0	10	10	0	0	0	0	0	6	3	0	0
S. ramosus	20	30	3	10	14	10	10	20	7	26	35	13	4	10
Spiniferites spp.	7	3	16	9	18	15	32	2	3	0	0	0	0	0
Tectatodinium pellitum	0	0	6	0	0	3	7	0	0	0	0	3	0	3
Tuberculodinium vancampoae	0	3	0	0	0	0	0	0	0	0	0	0	0	0
Acritarchs														
Cymatiosphaera globulosa	0	0	0	0	1	1	0	0	0	0	0	0	0	0

and 4 list the dinocyst data from both cores, but only core M9 (Fig. 6) is discussed here in detail. It is also important to note that the euryhaline planktonic foraminifer, *Globigerina quinqueloba*, is present throughout core M9 (Aksu et al., in prep.), which clearly establishes that the Marmara Sea was not a freshwater environment during the last glacial interval. Likewise, although the exact date of freshwater outflow from the Black Sea is not yet certain (see Aksu et al., 1999), the Marmara and Black seas were not connected before 11,000 yr BP.

Four lithofacies are identified in core M9 (Figs. 6 and 7). Facies D is a dark gray organic-rich mud deposited under conditions of moderate salinity (~18 ppt) and low summer sea surface temperature (Fig. 7). Dinocysts are abundant (~60,000 cm^{-3}), but

Table 3
Total numbers of palynomorphs and relative abundances of dinoflagellates in core M9 from Marmara Sea. Peridinioids include cysts of *Protoperidinium* and *Peridinium*; others are polykrikoids

Core M9: depth in cms	0	10	20	30	40	50	60	70	80	90	100	110	120	130	140	150	160	170	180	200	215
Total dinocysts/g × 100	6.1	15	46	15	11	7.2	7.2	11	19	22	19	30	15	15	23	17	12	20	56	22	61
Total acritarch/g × 100	0	0	6	8	12	20	26	11	16	23	40	50	24	33	23	72	66	45	40	32	7
Total *Pediastrum*/g	0	0	0	0	0	4	0	0	0	0	2	0	0	0	0	0	0	3	0	2	0
Total pollen-spores/g × 100	2.7	12	17	10	11	8.8	19	24	44.6	101	103	99	78	69	47	61	60	99	186	104	170
Dinocyst species																					
(A) Protoperidinioids																					
Brigantedinium spp.	0	0	15	8	10	0	0	2	0	3	2	0	3	3	0	0	0	0	0	0	0
Algidasphaeridium? *minutum*	10	6	0	0	0	0	0	0	0	0	2	0	0	0	0	0	0	0	0	0	0
Selenopemphix quanta	0	2	0	0	2	0	0	0	0	0	0	0	0	0	0	0	0	0	0	0	0
Pentapharsodinium dalei	0	2	2	2	0	0	0	0	0	0	0	0	0	0	0	0	0	0	0	0	0
P. ponticum	2	2	0	2	0	0	2	4	4	17	2	2	11	0	3	0	0	2	6	6	2
Pyxidinopsis spp.	0	0	0	4	0	0	0	0	0	0	0	4	0	3	0	4	8	3	3	0	0
S. stellatum	2	0	0	6	0	0	0	0	0	0	0	0	0	0	0	0	0	0	0	0	0
Trinovantedinium capitatum	0	4	3	0	0	0	0	0	0	0	0	0	0	0	0	0	0	0	0	0	0
Polykrikos spp.	2	2	8	0	0	0	0	0	0	0	2	0	0	0	0	0	0	0	0	0	0
(B) Gonyaulacoids																					
Ataxiodinium choane	0	0	0	0	0	0	0	0	0	0	0	0	0	0	0	0	0	0	0	2	0
Bitectatodinium tepikiense	0	0	0	0	0	0	0	2	0	0	0	0	0	0	0	0	0	3	0	2	0
Gonyaulax tamarensis	6	2	2	2	4	0	0	2	2	8	0	0	0	0	0	2	0	0	3	0	0
Lingulodinium machaerophorum	16	22	19	11	14	6	9	9	4	0	2	0	0	0	0	0	0	0	3	0	0
L. machaerophorum var. *clavatum*	2	6	2	0	0	4	0	0	0	0	0	0	0	0	0	0	2	0	0	0	3
Impagidinium aculeatum	0	2	0	0	0	0	0	0	0	0	0	0	0	0	0	0	0	0	0	0	0
Nematosphaeropsis labyrinthus	4	0	0	2	0	0	0	0	0	0	0	0	0	0	0	0	0	0	0	0	0
N. lemniscata	0	2	0	0	0	0	0	0	0	0	0	0	0	0	0	0	0	0	0	0	0
Operculodinium centrocarpum	20	12	6	2	8	0	2	6	2	0	2	0	0	0	0	0	0	0	3	0	0
O. centrocarpum var. *cezare*	2	0	6	2	10	0	0	0	0	0	0	0	0	3	0	0	0	0	0	0	0
O. centrocarpum var. *truncatum*	2	2	0	4	0	0	0	0	0	0	0	0	0	0	0	0	0	0	0	0	0
Polysphaeridium zoharyi	2	2	0	2	2	0	0	0	2	0	0	0	0	0	0	0	0	0	0	0	0
Spiniferites bentori	2	0	0	4	6	0	0	4	0	0	0	0	0	0	0	0	0	0	0	0	0
S. bulloideus	3	0	2	4	6	0	0	0	0	0	3	0	4	0	0	0	0	0	0	2	0
S. cruciformis	6	2	15	21	18	38	64	44	78	73	68	82	85	82	77	78	77	61	59	68	89
S. delicatus	0	0	0	0	0	0	0	0	0	0	0	2	0	0	0	0	0	0	0	0	0
S. mirabilis	4	14	6	7	2	2	2	4	0	0	0	0	0	0	0	0	0	0	0	0	0
S. ramosus	18	6	6	8	8	8	2	0	2	4	3	2	0	0	0	0	2	0	0	0	0
Acritarchs																					
Sigmopollis psilatum	0	0	6	8	12	20	26	11	16	23	40	50	24	33	23	72	66	45	40	32	7

only three species are present: *S. cruciformis* (89%, most of which are represented by forms 1 and 2), with traces of spheroidal cysts of *P. psilata* and *L. machaerophorum* with short clavate processes. This assemblage most closely resembles that in the *S. cruciformis–P. psilata* assemblage zone of the Black Sea.

Facies C in core M9 is a laminated sapropel unit (Figs. 6 and 7). Foraminiferal transfer functions and isotopic data show that the lower portion of this facies was deposited under low salinity (14–17 ppt) and low summer temperature (10°C) conditions. However, salinity estimates gradually rise to 21 ppt at the top of Facies C, with associated rise in summer SST to 14°C. Dinocyst concentrations in this glacial-stage sapropel are much lower (10,000–20,000 cysts cm^{-3}) than found in the Holocene sapropel (Facies B and Unit 2 in the Black Sea cores, but the assemblages are similarly dominated by *S. cruciformis* (59–86%) and *P. psilata* (3–22%). In the Marmara Sea, however, diversity is higher, with other species including *P. ponticum*, *Pyxidinopsis reticulata*, *L. machaerophorum* and traces of *Brigantedinium* spp., *B. tepikiense* and *O. centrocarpum*.

Facies B in the Marmara Sea core M9 is a silty mud, deposited under sea surface temperature and salinity conditions similar to the top of Facies C, but with a lower organic content than the sapropel. Dinocyst concentrations ($\sim$10,000 cm^{-3}) are also relatively low and *S. cruciformis* and *P. psilata* remain the dominant species. However, *L. machaerophorum* increases in this facies, and the common Mediterranean species *O. centrocarpum*, *S. bentorii* and *S. mirabilis* are occasionally present.

Facies A is a bioturbated brownish mud, similar the late Holocene sediment in core M97-2 but with a lower organic content. Temperature estimates are slightly higher than in Facies B and SSS remains at about 21 ppt. Dinocyst concentrations are low as in Facies B, but there is a large change in the flora because of a sharp decrease in the percentage of *S. cruciformis* and *P. psilata*, with corresponding increases in *L. machaerophorum*, *O. centrocarpum* and euryhaline *Spiniferites* species. Traces of *P. zoharyi* and *N. labyrinthus* are present, indicating inflow of warm, saline Mediterranean and North Atlantic water, which places the age of Facies A at $<$11,000 yr BP, the time at which the Strait of Dardanelles was fully overtopped by rising sea level (Aksu et al., 1999). This assemblage zone is also marked by the appearance of protoperidinioids, *B. simplex*, *Selenopemphix quanta*, *Algidasphaeridium*? *minutum*, and by the presence of *Polykrikos* spp. This *Brigantedinium–O. centrocarpum–Brigantedinium* dinocyst zone is similar to the low salinity dinocyst zone at the top of the Black Sea cores but differs in the near-absence of *P. ponticum* and the presence of the Mediterranean and North Atlantic species. In this respect, the youngest zone in M9 more closely resembles the late Holocene and modern dinocyst flora in M97-2 (see Table 4). It is also notable that *Cymatiosphaera globulosa* was not observed in any samples from Marmara Sea. This suggests that there was no transport of 'Old Black Sea' brackish water (see Fig. 4) into the Marmara Sea from $\sim$7000–3000 yr BP. Alternatively, early-mid Holocene sediments may be absent in cores M9 and M97-2.

3.4. Numerical analysis of variation with salinity

The SSS data for core M9 (Fig. 7) are from the same sample intervals as the dinocyst assemblage data, so they can be used to examine the numerical relationship between salinity and relative abundances of cyst morphotypes. Percentage abundances were used for the graphs rather than total abundance, because there is little variation in cyst abundance/g in core M9 (see Fig. 7) so that abundance and percentage data record the same responses to salinity. Moreover, it seemed more useful to work with relative abundances because most pre-Quaternary data and petroleum exploration palynology data are reported as relative abundances (e.g. $>30\%$ = abundant, $<5\%$ = rare, etc.). Correlation between percent abundance and salinity was tested using R, the standard Pearson product-moment coefficient.

Fig. 8 shows the relationship between surface water salinity and percentage abundance of *L. machaerophorum* for two distinctive morphotypes from the study region (Plate 2): (A) the normal form which has long ($>$15 μm) flexuous (or, rarely, straight) processes and tapered or pointed tips bearing small spinules, and (B) a smaller form with short linear or conical processes ($<$5–10 μm) and truncated or clavate tips. Statistical analysis of the combined data

Table 4
Total numbers of palynomorphs and relative abundances of dinoflagellates in Core M97-2 from Marmara Sea. Peridinioids include cysts of *Protoperidinium* and *Peridinium*; others are polykrikoids and gymnodinioids

Core M97-2: depth in cm	0	10	20	30	40	50	60	70	80	90	100	110	120	130	140	150	160	170	180	220
Total dinocysts/g × 100	2.7	4.5	3	2.5	2.6	3.5	3.5	7.6	4.1	3.9	4.2	2.8	12	4.7	6.3	9.3	28	14	6.8	4.3
Total acritarch/g × 100	1	0	0	0	3	3	0	0	0	0	0	0	0	0	0	2	0	0	0	0
Total fungal spores/g	0	6	0	6	0	1	1	0	0	0	0	0	0	4	0	2	0	1	5	0
Total pollen-spores/g × 10	5.8	6.1	2.7	1.5	3	2.2	2.7	1.8	0.7	1.3	0.8	0.8	3.4	1.1	1.2	4.6	14	8.9	7	2.2
Pre-Quaternary cysts/g	16	0	30	42	12	32	23	0	14	26	15	0	0	63	19	39	56	46	45	0
Dinocyst species																				
(A) Protoperidinioids																				
Brigantedinium spp.	20	26	67	30	29	58	23	30	27	7	9	43	25	13	22	79	50	65	60	50
Dinocyst spp. of Wall et al. 1977	0	0	3	10	2	0	0	0	0	0	1	0	0	3	2	0	0	0	0	0
Echinidinium spp.	9	6	20	7	2	2	7	0	7	7	2	17	16	20	0	0	0	0	7	0
Gymnodinium spp. cf. *catenatum*	0	0	0	0	0	2	0	0	0	0	0	0	0	3	0	0	0	0	0	0
Lejeunecysta oliva	0	0	0	0	0	0	0	0	0	0	0	0	0	0	1	0	0	0	0	0
Algidasphaeridium? minutum	0	0	0	3	0	0	0	0	0	0	2	0	0	0	0	0	0	0	0	0
Multispinula quanta	9	4	3	3	5	4	10	7	7	7	1	3	0	0	2	0	0	0	0	4
Pentapharsodinium dalei	2	0	0	0	0	0	0	0	0	0	0	0	0	0	0	0	0	0	0	0
P. ponticum	0	0	0	0	2	4	0	0	0	0	0	0	0	0	1	0	0	0	3	0
Quinquecuspis concretam	2	0	0	0	0	0	0	0	3	0	0	0	0	0	1	0	0	0	0	0
Selenopemphix nephroides	2	2	3	3	7	2	13	0	0	0	2	3	0	0	0	0	2	3	0	6
S. stellatum	4	0	0	0	2	4	10	0	13	10	9	0	0	3	2	4	8	3	7	2
Trinovantedinium applanatum	0	0	0	0	0	0	0	0	0	0	4	0	0	0	0	0	0	0	0	0
Votadinium calvum	2	0	0	0	0	0	0	0	0	0	0	0	0	0	0	0	2	0	0	0
Xandarodinium variabile	0	0	0	0	0	0	0	0	0	3	0	0	0	0	1	0	0	0	0	0
Polykrikos kofoidii	0	16	0	0	7	0	3	0	7	7	0	3	0	0	0	0	0	0	0	0
P. schwartzii	0	0	10	7	0	0	0	0	0	0	0	0	0	0	0	0	0	2	0	0
(B) Gonyaulacoids																				
Bitectatodinium tepikiense	2	0	0	0	0	0	0	0	0	0	0	0	0	0	0	0	0	0	0	0
Gonyaulax tamarensis	0	0	0	0	1	0	1	0	1	0	0	0	0	0	0	0	0	0	0	0
Lingulodinium machaerophorum	9	2	3	0	2	2	0	7	0	0	3	0	0	3	8	0	4	3	0	6
L. machaerophorum var. *clavatum*	0	0	0	0	0	0	0	0	0	0	1	3	0	0	1	0	0	0	0	2
Operculodinium centrocarpum	7	4	17	10	7	2	3	3	10	3	8	10	0	7	10	0	2	0	7	4
O. centrocarpum var. *cezare*	7	0	0	0	2	0	7	0	0	0	0	4	3	6	0	1	0	0	0	0
O. centrocarpum var. *truncatum*	2	2	0	4	0	0	0	0	0	0	0	0	0	0	0	0	0	0	0	0
Spiniferites bulloideus	0	2	0	0	0	2	0	0	0	0	4	0	3	3	1	0	0	0	0	0
S. cruciformis	0	0	0	0	0	0	0	0	0	0	0	0	0	1	0	0	0	0	0	2
S. mirabilis	4	2	0	3	2	2	0	0	7	3	0	0	0	0	4	0	0	0	0	0
S. ramosus	7	14	20	10	7	8	23	20	13	27	22	10	13	20	32	13	6	3	7	17
Spiniferites spp.	0	2	0	0	7	0	0	13	0	9	0	6	0	1	0	0	0	0	0	2
Tectactodinium pellitum	0	0	0	3	0	2	0	0	0	0	0	0	0	0	0	0	0	0	0	0

Table 4 (*continued*)

Core M97-2: depth in cm	0	10	20	30	40	50	60	70	80	90	100	110	120	130	140	150	160	170	180	220
T. psilatum	0	0	0	0	0	0	0	10	0	0	4	0	0	3	2	0	0	3	0	0
Acritarchs																				
Beringiella spp.	0	2	7	0	0	15	7	3	0	7	2	7	0	0	2	8	0	0	0	0
Concentrites spp.	1	0	0	0	1	0	0	0	0	0	0	0	0	0	0	0	0	0	0	0
Cyst C (copepod egg?)	0	0	0	3	0	0	7	0	3	3	3	0	3	0	0	8	0	0	0	0
Sigmopollis psilatum	0	0	0	0	1	1	0	0	0	0	0	0	0	0	0	0	0	0	0	0

from Fig. 8A and B (not shown on a separate graph) reveals a weak correlation ($R = 0.71$) between the percentage of *L. machaerophorum* (all forms) and increasing salinity between 16 and 21.5 ppt. However, there is no clear relationship ($R = 0.33$) between process length or shape and salinity: 'clavate' forms comprise 66–10% of the *L. machaerophorum* population between 20 and 21 ppt and 100% in two samples with salinities of 16–17 ppt. By comparison, the 'normal' form comprises 0–100% of the population at salinities less than 20 ppt. The same results are obtained by converting the percentage abundances to abundance per cubic centimeter, using the data in Table 2.

The relationship between morphology and salinity in the stenohaline species *S. cruciformis* (Fig. 9) is also complex. When all forms are grouped (Fig. 9F), there is a weak negative correlation between percentage of *S. cruciformis* (sensu lato) and salinity ($R = -0.61$) in the range from 14.5 to 21.5‰. *S. cruciformis* form 1 also shows weak negative correlations ($R = -0.67$) between abundance and salinity (Fig. 9A), with the degree of velum development apparently decreasing with reduction in salinity. In contrast, *S. cruciformis* forms 3, 4 and 5 show no clear correlation ($R = <0.37$) with salinity (Fig. 9B and D) except for the tendency of the most reduced form, *S. cruciformis* form 5, to be clustered at the lowest (14–16‰) and highest (21–22‰) ends of the salinity range. This tendency may also be present in the distribution of clavate cysts of *L. machaerophorum* (Fig. 8B) but it is less clear because of the fewer samples with this tax on.

4. Discussion

In their pioneer work on dinocysts from Holocene sediments in the Black Sea, Wall et al. (1973) and Wall and Dale (1974) noted the presence of a relatively large number of taxa with cruciform or pyriform central bodies and with variable process length or shape. They suggested that these variations reflected responses to low salinity or other environmental stress. The idea that process length varies with salinity was later supported by studies of *L. machaerophorum*, *O. centrocarpum* and several non-cruciform *Spiniferites* species in Norwegian fiords and the Baltic

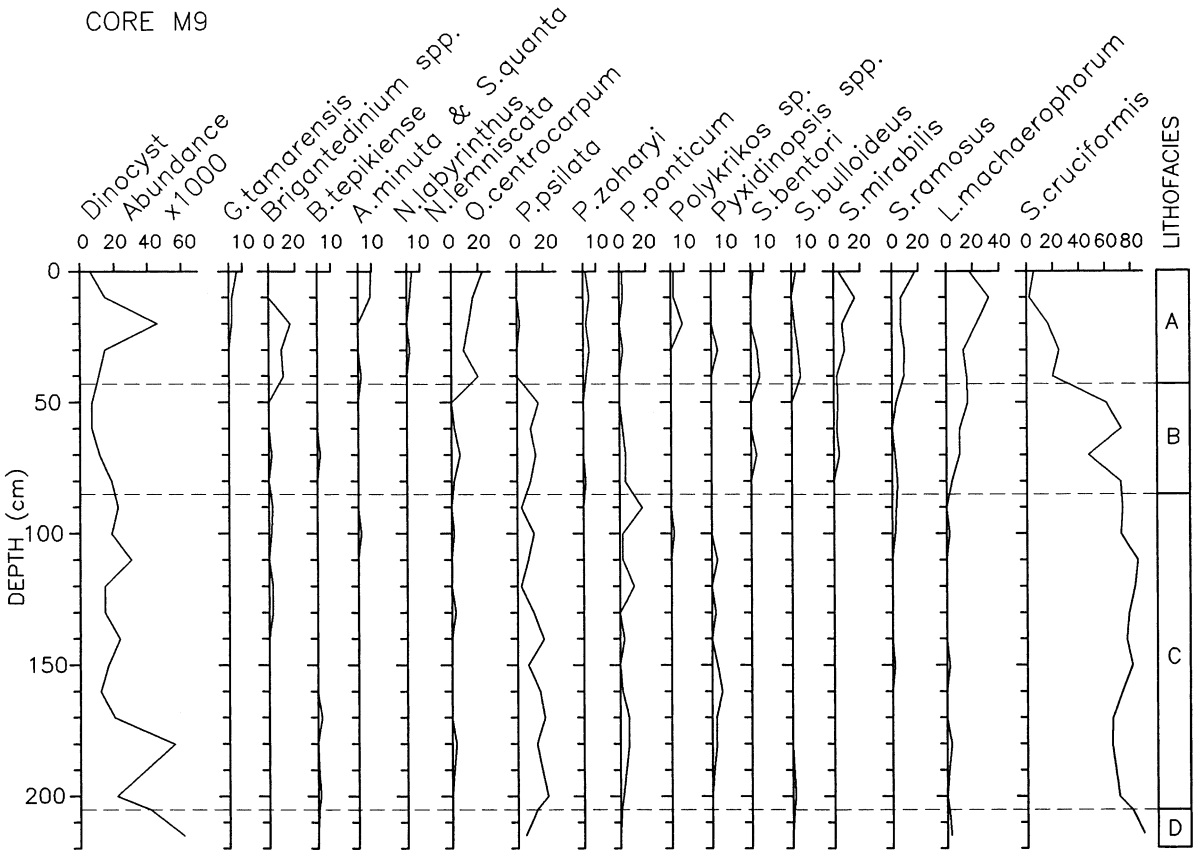

Fig. 6. Marmara Sea core M9, showing lithofacies, dinocyst abundance cm^{-3} and percentage abundance of the main species.

Sea (Dale, 1996; Nehring, 1994; Matthiessen and Brenner, 1996) and in eastern Canadian fiords or channels (Mudie, 1980, 1992). A large range of cyst size and process length in *Spiniferites bulloideus*, *L. machaerophorum* and *O. centrocarpum* was also described for a sediment core from Limfjord, Denmark, near the North Sea entrance to the Baltic Sea by Ellegaard (2000) who attributed these morphological variations to changes in salinity, although no salinity data were actually given for the core site. Large variations in process length were also noted in *O. centrocarpum* and *Algidasphaeridium*? *minutum* from low salinity environments of glacial Lake Champlain (de Vernal et al., 1989) where microfaunal data indicated bottom water values of 15–30 ppt. A cruciform (biconical) *Achomosphaera* species was reported (Demetrescu, 1989) for the early Pliocene of southwest Romania which was probably a brackish water lake at that time. Cruciform cysts and supercavate cyst-forms (*Seriliodinium explicatum*), and a supercavate cystform (*Thalassiphora*-like cysts) have been described from hard, pale gray mudstone of Pliocene to mid-Pleistocene age in the Black Sea (Eaton, 1996) where they constituted about 11% of all dinocysts, including reworked Cretaceous and Miocene taxa. Most recently, *S. cruciformis*, including morphotypes resembling the forms 1–3 described in this paper, has been found in late-glacial sediment from a freshwater mountain lake in Northern Greece (Kouli et al., 2001). The disappearance of *S. cruciformis* by the mid-Holocene in the Greek lake reenforces and extends the original interpretation of Wall et al. (1973) that *S. cruciformis* is a cool water, low salinity stenohaline species which was common

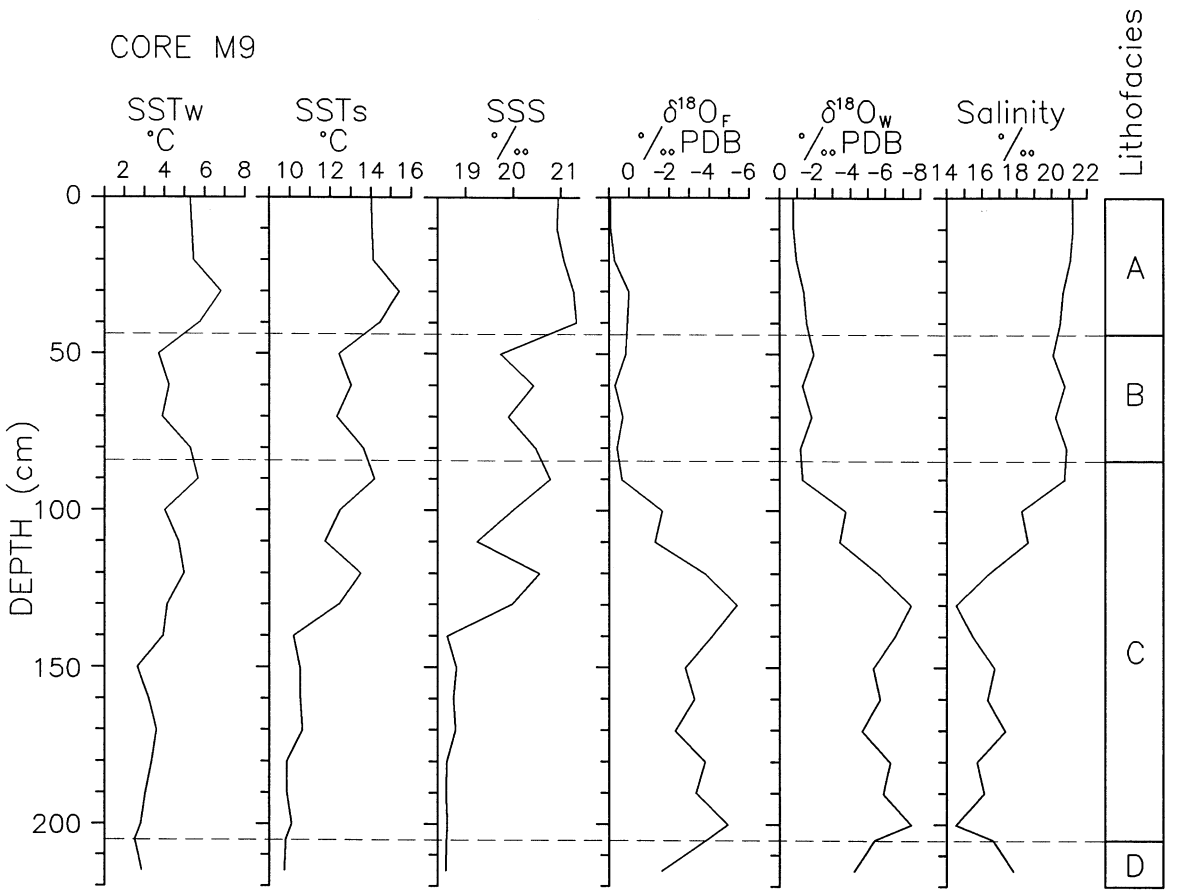

Fig. 7. Marmara Sea core M9, showing lithofacies, foraminiferal transfer function SST for winter (w) and summer (s) and salinities (SSS) for winter, oxygen isotopic data ($^{18}O_F$) from *N. quinqueloba*, estimates of the oxygen isotopic composition of the surface waters ($^{18}O_w$; discussed in text), and the surface water salinity estimates calculated using the relationship between the $^{18}O_w$ and salinity in the Marmara Sea. Salinity is shown as parts per thousand (‰).

in late-glacial to early Holocene sediments of the eastern Mediterranean region, but failed to survive the postglacial influx of saline water and/or increase in temperature.

These and other studies (Dale, 1996, 1988) have led to the hypothesis that cruciform body shape and/or reduced processes in cysts may be indicators of low salinity (fresh water to brackish estuarine) environments. In laboratory experiments, Lewis and Hallett (1997) also found that cysts of *L. machaerophorum* had shorter spines at lower salinities when cultured in a range of salinity from 10–40 ppt. Other experiments with *L. machaerophorum* (Kokinos and Anderson, 1995) and with *Spiniferites membranaceus* and *S. ramosus* (Lewis et al., 1999), however, have shown that the full range of process length development and ornament can be found in cysts grown from single cell cultures, without any change in salinity conditions. These laboratory studies suggest that major variations in process length may reflect arrested development of process expansion in response to environmental stresses that can include salinity, but are not confined to that parameter. For example, it is also known that most motile dinoflagellates are extremely sensitive to wind- and wave-induced turbulence (Thomas et al., 1995; Zirbel et al., 2000) and cyst production in *L. machaerophorum* is also negatively affected by turbulence (Blanco, 1995).

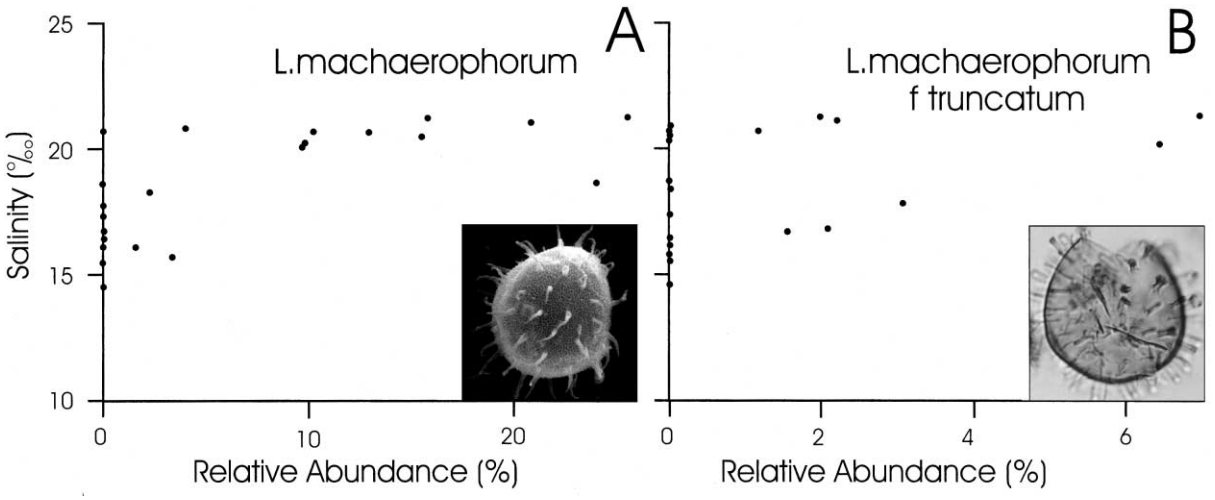

Fig. 8. Relationship between surface salinity estimates in ppt (‰) and relative abundances of (A) *L. machaerophorum* and (B) *L. machaerophorum* 'truncate' form in M9.

Zirbel et al. (2000) showed that *Ceratocorys horrida* changed from forms with long spines to spineless in response to increased in turbulence, with individual cells regulating their cell size over a period of hours. The smaller short-spined cells produced under turbulent conditions had a sinking rate up to about 30% faster than the long-spined forms (Zirbel et al., 2000). This apparent adaptive response to turbulence differs from that involved in formation of small-cell populations under conditions of nutrient exhaustion (Silva and Faust, 1995): here total size decreases after cell division, but there is no change in either body shape or in process length relative to body diameter.

These laboratory findings are consistent with our field data that show there is not a simple relation between process development and salinity in the range of ~7–22 ppt. However, some of our field data show a tendency for the end-point morphologies (i.e. the most- and least-developed processes) to be most abundant at the ends of the salinity ranges. For example, *S. cruciformis* forms 1 and 2 are dominant at the lowest salinities (and in freshwater lakes according to Kouli et al., 2001), while the spineless form 5 is most common at the upper limit of its salinity (~21 ppt) and was not recorded for the freshwater lake. This feature seems in agreement with the fact that cell growth in cultures of *G. tamarense* is curtailed at the extremes of a growth-medium salinity gradient from 10 to 30 ppt (Parkhill and Cembella, 1999). The role of turbulence in shaping cyst morphology is presently unknown, but experimental evidence suggests that cysts with reduced processes and higher sinking rate (e.g. Anderson et al., 1985; Sargeant et al., 1987) would be at a disadvantage in a stratified deep-water environment where they would sink out of resuspension range.

In the late Pleistocene sediments of the eastern Mediterranean marginal seas, high percentages of species with cruciform body shapes are confined to glacial-stage or early post-glacial assemblages with paleosalinities of less than 22 ppt. Absence of the cruciform species, *S. cruciformis*, from late Holocene and modern marine and lake sediments may also indicate a low temperature tolerance for this taxon. It is notable, however, that cruciform species or morphotypes (e.g. *P. psilata*) are not found in modern cold, low salinity (<3 ppt) environments, e.g. the eastern Baltic Sea and inner Norwegian fiords (Dale, 1996). In fact, all known species with cruciform endocysts appear to be restricted to the glacial-early postglacial sediments of the eastern Mediterranean region, and the Quaternary species seem to occur only in the glacial-early postglacial interval. This restricted geographic distribution of cruciform species may indicate that following its probable origin in the Pliocene (Eaton, 1996), the hyposaline cruciform dinoflagellate lineage has not been able to spread

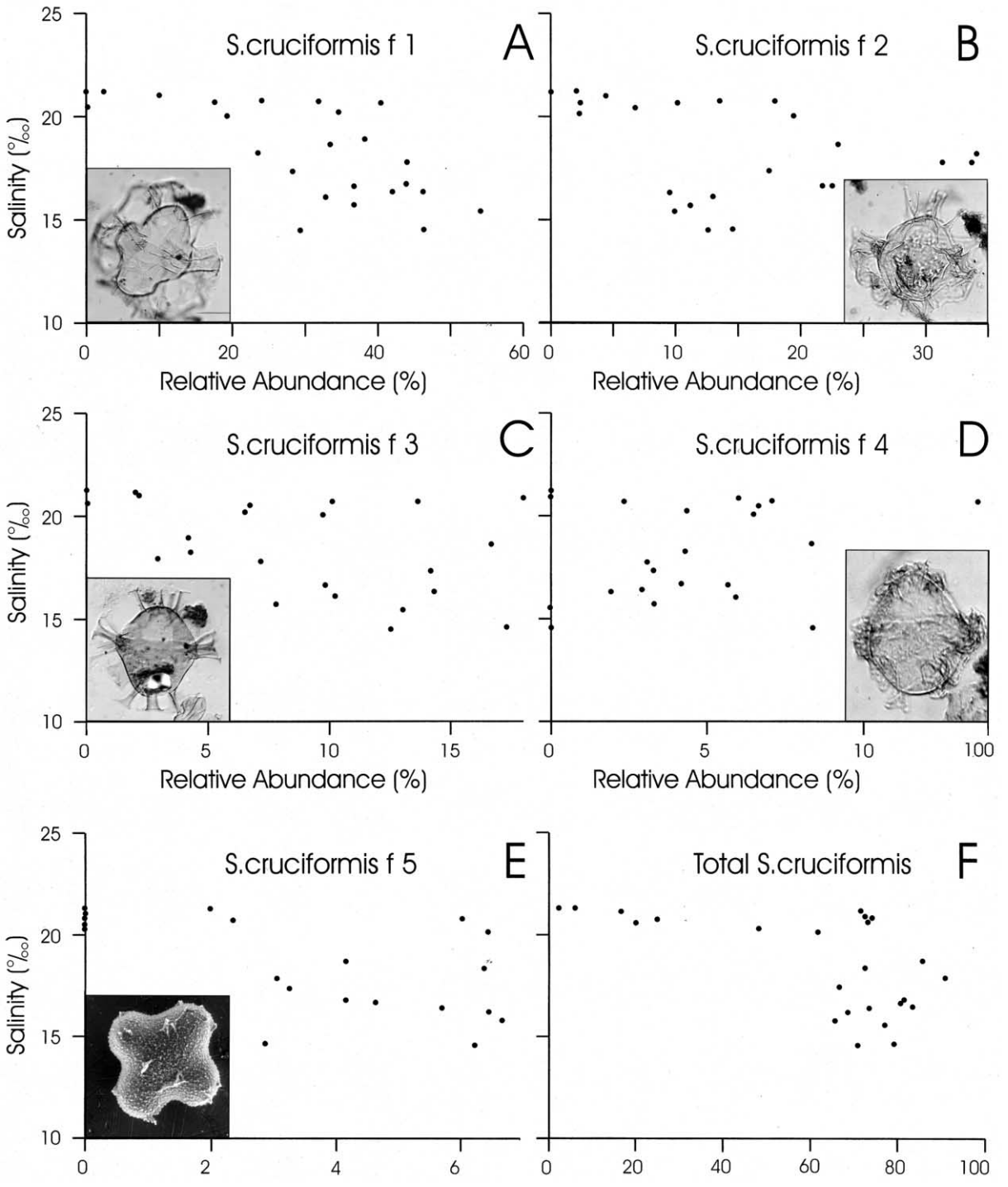

Fig. 9. Relationship between surface water salinity estimates in ppt (‰) and relative abundances of morphotypes of *S. cruciformis* in Core M9.

beyond the eastern Mediterranean region because of its inability to transgress saline marine barriers.

In general, the available data suggest that the following paleoenvironmental conditions may be inferred from the assemblages described in this paper:

1. Very low diversity assemblages ($S = 2$–3) of gonyaulacoid species dominated by cysts with strongly cruciform cyst bodies and inflated septa (*S. cruciformis–P. psilata* assemblage) indicates quasi-freshwater (<7 ppt), well-mixed environments with winter temperatures of 2–3°C and summer temperatures of ~10°C (a similar summer temperature was inferred for the low diversity Greek lake *S. cruciformis–Gonyaulax apiculata* assemblage by Kouli et al., 2001).
2. More diverse assemblages ($S = 8$–10) with ~10% cruciform species and at least 10% of forms with reduced processes are indicative of warmer SST for winter (4–6°C) and summer (12–14°C) and more saline (>10–14 ppt), probably strongly stratified paleoenvironments. The late glacial Marmara Sea data for Unit C in Core M9 clearly show that *S. cruciformis* lived in salinities from 14–20 ppt, as well as in the very low salinities (3.5–7 ppt) of the Black Sea 'freshwater' Euxinic Stage. The possibility of long distance transport of cruciform cysts from the Black to the Marmara seas is not valid for these deposits pre-date the opening of the Bosphorus Strait.
3. Diverse ($S = >10$) assemblages of gonyaulacoid Mediterranean and Atlantic species are associated with salinities of >37 ppt and summer temperatures >14°C in the Aegean Sea. Most of these salt tolerant taxa have reduced septal membranes. Rare cruciform cysts are found only in the mid-Holocene organic sediments and were probably transported from the Black and Marmara seas during floodwater events. Some of the hypersaline species and morphotypes with reduced processes are also common in late Holocene sediments of Marmara Sea, deposited beneath brackish surface water (22 ppt) which is formed by mixing of Black Sea and Mediterranean water (see Tables 3 and 4, and Aksu et al., 1999), but here *Impagidinium* species are absent.

5. Conclusions

- Cores from the southeastern Black Sea have early Holocene *S. cruciformis–P. psilata* assemblages corresponding to salinities of <7 ppt but probably not entirely fresh water.
- Glacial-late glacial facies in eastern Marmara Sea cores have *S. cruciformis–P. psilata–P. ponticum* assemblages corresponding to salinities of ~14–20 ppt. The abundance of *S. cruciformis* remains high during the gradual increase of salinity, indicating a much wider range of salinity tolerance than previously reported.
- Aegean sapropels with salinities of ~36–37 ppt have common *L. machaerophorum* and traces of *S. cruciformis* and *P. psilata* probably transported by strong overflow of Black Sea water.
- Percentage abundance of the normal form of *L. machaerophorum* is weakly correlated with salinity from 20–21 ppt, and morphotypes with reduced processes tend to be clustered at the limits of the salinity range.
- In Marmara Sea, 40–60% of *S. cruciformis* cysts have long processes and expanded membranous septa (forms 1 and 2), and abundances of *S. cruciformis* form 1 are negatively correlated with salinity. Morphotypes with highly reduced processes (form 5) tend to occur at the salinity limits, while intermediates (forms 2, 3 and 4) show no definite trend.

Acknowledgements

We thank Prof. Dr Orhan Uslu, the Director of the Institute of Marine Sciences and Technology, for his support and encouragement. We extend our special thanks to the officers and crew of the RV *Koca Piri Reis* for their assistance in data acquisition, in particular Captain Mehmet Özsayg l and Chief Engineer Ömer Çubuk. We thank Allison Pye and Adrian Timbal for their assistance in stable isotopic determinations. We acknowledge research funds from the Natural Sciences and Engineering Research Council of Canada (NSERC) to Aksu (OGP0042760), ship-time funds from NSERC to Aksu and Hiscott (MIS0180897 and MIS0184640), and Geological

Survey of Canada funding for project 920063 of Mudie. Jens Matthiessen of the Alfred Wegener Institute, Bremerhaven, and Martin Head, Department of Geography, Cambridge University, critically read the manuscript and provided many valuable comments.

References

Aksu, A.E., Yasar, D., Mudie, P.J., 1995a. Paleoclimatic and paleoceanographic conditions leading to development of sapropel layer S1 in the Aegean Sea basins. Palaeogeogr. Palaeoclimatol. Palaeoecol. 116, 71–101.

Aksu, A.E., Yasar, D., Mudie, P.J., Gillespie, H., 1995b. Late glacial–Holocene paleoclimatic and paleoceanographic evolution of the Aegean Sea: micropaleontological and stable isotopic evidence. Mar. Micropaleontol. 25, 1–28.

Aksu, A.E., Yasar, D., Mudie, P.J., 1995c. Origin of late glacial-Holocene sediments in the Aegean Sea: clay mineralogy and carbonate sedimentation. Mar. Geol. 123, 33–59.

Aksu, A.E., Hiscott, R.N., Yasar, D., 1998. Oscillating Quaternary water levels of the Marmara Sea and vigorous outflow into the Aegean Sea from the Marmara Sea–Black Sea drainage corridor. Mar. Geol. 153, 275–302.

Aksu, A.E., Hiscott, R.N., Yasar, D., Mudie, P.J., 1999. Deglacial and postglacial water levels and water exchange across the Black Sea–Marmara–Aegean Sea shelves, Eastern Mediterranean region. Proceedings of the Emery Commemorative Workshop on Land-Sea Links in Asia, Tsukuba, Japan.

Anderson, D.M., Lively, J.J., Reardon, E.M., Price, C.A., 1985. Sinking characteristics of dinoflagellate cysts. Limnol. Oceanogr. 27 (30), 1000–1009.

Blanco, J., 1995. Cyst production in four species of neritic dinoflagellates. J. Phytoplankton Res. 17, 165–182.

Crusius, J., Anderson, R.F., 1992. Inconsistencies in accumulation rates of Black Sea sediments from records of laminae and ^{210}Pb. Paleoceanography 7, 215–227.

Dale, B., 1988. Low salinity dinoflagellate cyst assemblages from Recent sediments of the Baltic region. Abstracts of the Seventh International Palynological Congress, Brisbane, Australia, 28 August–2 September 1988, p. 33.

Dale, B., 1996. Dinoflagellate cyst ecology: modelling and geological applications. In: Jansonius, J., McGregor, D.C. (Eds.), Palynology: Principles and Applications. Am. Assoc. Strat. Palynol. Found., Salt Lake City, Utah 3, 1249–1275.

Demetrescu, E., 1989. *Achomosphaera argesensis*: a new dinoflagellate species from the early Pliocene of the southern Carpathians foredeep, Romania. Rev. Palaeobot. Palynol. 59, 51–55.

Deuser, W.G., 1972. Late-Pleistocene and Holocene history of the Black Sea as indicated by stable isotope studies. J. Geophys. Res. 77, 1071–1077.

Duman, M., 1992. Late Quaternary evolution of the southern Black Sea basin. PhD thesis, Institute of Marine Sciences and Technology, Dokuz Eylül University, pp. 1–101.

Duman, M., 1994. Late Quaternary chronology of the southern Black Sea Basin. Geo. Mar. Lett. 14, 272–278.

Eaton, G.L., 1996. *Seriliodinium*, a new late Cenozoic dinoflagellate from the Black Sea. Rev. Palaeobot. Palynol. 91, 151–169.

Ellegaard, M., 2000. Variations in dinoflagellate cyst morphology under condition of changing salinity during the last 2000 years in Limfjord, Denmark. Rev. Palaeobot. Palynol. 109, 65–81.

Harland, R., 1977. Recent and late Quaternary (Flandrian and Devensian) dinoflagellate cysts from marine continental shelf sediments around the British Isles. Palaeontogr. Abt. B 164, 87–126.

Head, M.J., 1994. A forum on Neogene and Quaternary dinoflagellate cysts: the edited transcript of a round table discussion held at the third workshop on Neogene and Quaternary dinoflagellates; with taxonomic appendix. Palynology 17, 201–239 Imprinted 1993.

Jones, G.A., Gagnon, A.R., 1994. Radiocarbon dating of Black Sea sediments. Deep Sea Res. 41, 531–557.

Kokinos, J., Anderson, D.M., 1995. Morphological development of resting cysts in cultures of the marine dinoflagellate *Lingulodinium polyedrum* (= *L. machaerophorum*). Palynology 19, 143–166.

Kouli, K., Brinkhuis, H., Dale, B., 2001. *Spiniferites cruciformis*: a fresh water dinoflagellate cyst? Rev. Palaeobot. Palynol. 113, 273–286.

Lewis, J., Hallett, R., 1997. *Lingulodinium polyedrum* (*Gonyaulax polyedra*), a blooming dinoflagellate. Oceanogr. Mar. Biol. Ann. Rev. 35, 97–161.

Lewis, J., Rochon, A., Harding, 1999. Preliminary observations of cyst-theca relationships in *Spiniferites ramosus* and *Spiniferites membranaceus* (Dinophyceae). Grana 38, 113–124.

Matthiessen, J., Brenner, W., 1996. Chlorococcalalgen und dinoflagellaten-zysten in rezenten sedimenten des greifswalder boddens (sudliche Ostsee). Senckenbergiana Maritima 27, 33–48.

McCarthy, F.M.G., Mudie, P.J., 1996. Palynology and dinocyst biostratigraphy of Upper Cenozoic sediments from ODP Leg 149 Sites 898 and 900, Iberian Abyssal Plain. In: Whitmarsh, R.B., Sawyer, D.S., Klaus, A., Masson, D.G. (Eds.), Proc. ODP, Sci. Results, 149, 241–265.

Morzadec-Kerfourn, M.T., 1986. Les kystes de dinoflagelles dans les sediments Pleistocenes superieurs et Holocenes au large du delta du Rhoneet de la Corse. In: Bizon, J.J., Burollet, P.F. (Eds.), Ecologie des Microorganismes en Mediterranee occidentale ECOMED, Vol.1. l'Assoc. Francaise de Technicienes du Petrole, Paris, pp. 170–183.

Mudie, P.J., 1980. Palynology of later Quaternary marine sediments, eastern Canada. PhD Thesis, Dalhousie University, pp. 1–638.

Mudie, P.J., 1982. Pollen distribution in marine sediments, eastern Canada. Can. J. Earth Sci. 19, 729–747.

Mudie, P.J., 1992. Circum-arctic Quaternary and Neogene marine palynofloras: paleoecology and statistical analysis. In: Head, M.J., Wrenn, J.H. (Eds.), Neogene and Quaternary dinoflagellate cysts and acritarchs. Am. Assoc. Strat. Palynol. Found, College Station, TX, pp. 347–390.

Nehring, S., 1994. Spatial distribution of dinoflagellate resting cysts

in Recent sediments of Kiel Bight, Germany (Baltic Sea). Ophelia 39, 137–158.

Parkhill, J-P., Cembella, A.D., 1999. Effects of salinity, light and inorganic nitrogen on growth and toxigenicity of the marine dinoflagellate *Alexandrium tamarense* from northeastern Canada. J. Plankton Res. 21, 939–955.

Rochon, A., de Vernal, A., Turon, J.-L., Matthiessen, J., Head, M.J., 1999. Distribution of dinoflagellate cysts in surface sediments from the North Atlantic Ocean and adjacent basins, and quantitative reconstruction of sea-surface parameters. Am. Assoc. Strat. Palynol. Found. Contrib. Ser. 35, 250 pp.

Ross, D.A., Degens, E.T., MacIlvaine, J., 1970. Black Sea: recent sedimentary history. Science 170, 163–165.

Sargeant, W.A.S., Lacalli, T., Gaines, G., 1987. The cysts and skeletal elements of dinoflagellates: speculations on the ecological causes for their morphology and development. Micropaleontology 33, 1–36.

Shackleton, N.J., 1974. Attainment of isotopic equilibrium between ocean water and benthic foraminifera genus *Uvigerina*: isotopic changes in ocean during the last glacial. Cent. Natl. Rech. Sci. Coll. Int. 219, 203–209.

Silva, E.S., Faust, M.A., 1995. Small cells in the life history of dinoflagellates (Dinophyceae): a review. Phycologia 34, 396–408.

Simard, A., de Vernal, A., 1998. Distribution des kystes du type *Alexandrium excavatum* dans les sediments recents et postglaciaires des marges est-Canadiennes. Géog. Phys. Quat. 52, 361–371.

Thomas, W.H., Vernet, M., Gibson, C.H., 1995. Effects of small-scale turbulence on photosynthesis, pigmentation, cell division, and cell size in the marine dinoflagellate *Gonyaulax polyedra* (Dinophyceae). J. Phycol. 31, 50–59.

Thunell, R.C., 1979. Eastern Mediterranean Sea during the last glacial maximum: an 18,000 years BP reconstruction. Quat. Res. 11, 353–372.

Turon, J.-L., Londeix, L., 1988. Les assemblages des kystes de dinoflagelles en Mediterranee occidental (Mer d'Alboran) mise en evidence de l'evolution des paleoenvironnements depuis le dernier maximum glaciaire. Bull. Centres Rech. Explor.-Prod. Elf-Aquitaine 12, 313–344.

de Vernal, A., Goyette, C., Rodrigues, C.G., 1989. Contribution palynostratigraphique (dinokystes, pollen et spores) à la connaissance de la mer de Champlain: coupe de SaintCezaire, Québec. Can. J. Earth Sci. 26, 2450–2464.

Wall, D., Dale, B., 1966. Living fossils in western Atlantic plankton. Nature 211, 1025–1026.

Wall, D., Dale, B., 1973. Paleosalinity relationships of dinoflagellates in the late Quaternary of the Black Sea — a summary. Geosci. Man VII, 95–102.

Wall, D., Dale, B., 1974. Dinoflagellates in late Quaternary deep-water sediments of Black Sea. In: Degens, E.T., Ross, D.A. (Eds.), The Black Sea — Geology, Chemistry and Biology. Mem. Am. Assoc. Petrol. Geol. 20, 364–380.

Wall, D., Dale, B., Harada, K., 1973. Descriptions of new fossil dinoflagellates from the late Quaternary of the Black Sea. Micropaleontology 19, 18–31.

Wall, D., Dale, B., Lohmann, G.P., Smith, W.K., 1977. The environmental and climatic distribution of dinoflagellate cysts in modern marine sediments from regions in the North and South Atlantic Oceans and adjacent seas. Mar. Micropaleontol. 2, 121–200.

Williams, G.L., Lentin, J.K., Fensome, R.A., 1998. The Lentin and Williams index of fossil dinoflagellates. Am. Assoc. Strat. Palynol. Found. Contrib. Ser. 34, 817 pp.

Zirbel, M.J., Veron, F., Latz, M.I., 2000. The reversible effect of flow on the morphology of *Ceratocorys horrida* (Peridiniales, Dinophyta). J. Phycol. 36, 46–58.

Zonneveld, K.A.F., 1995. Paleoclimatical and palaeo-ecological changes during the last deglaciation in the eastern Mediterranean; implications for dinoflagellate ecology. Rev. Palaeobot. Palynol. 84, 221–253.